European Journal of Taxonomy 1039: 297–322
https://doi.org/10.5852/ejt.2026.1039.3197

europeanjournaloftaxonomy.eu
ISSN 2118-9773
2026 · Voet I. *et al.*

Received: 28 August 2025 • Accepted: 12 December 2025 • Published: 17 February 2026

Topic editor: Magalie Castelin • Desk editor: Lizeth Alonso

Research article

urn:lsid:zoobank.org:pub: urn:lsid:zoobank.org:pub:529908CA-29A5-4F37-8BF9-4208B245CDE0

Integrative taxonomy resolves a new West African *Crocidura* (Mammalia: Soricidae) species, cryptic to *Crocidura grandiceps* in color, but distinct in size

Inessa VOET [1], Arnaud DELAPRÉ [2], Christiane DENYS [3], Aude LALIS [4], Raphaël CORNETTE [5, a] & Violaine NICOLAS [6, a, *]

[1,2,3,4,5,6] Institut de Systématique, Evolution, Biodiversité (ISYEB), Muséum national d'Histoire naturelle, CNRS, Sorbonne Université, EPHE-PSL, Université des Antilles, CP51, 57 rue Cuvier, 75005 Paris, France.
[1] Naturalia Environnement, 60 rue Jean Dausset, 84000 Avignon, France.
[a] co-last authors

[*] corresponding author: violaine.colin@mnhn.fr
[1] Email: i.voet@naturalia-environnement.fr
[2] Email: arnaud.delapre@mnhn.fr
[3] Email: christiane.denys@mnhn.fr
[4] Email: aude.lalis@mnhn.fr
[5] Email: raphael.cornette@mnhn.fr

Abstract. High species richness in tropical West Africa has been demonstrated for many species groups, among which shrews are no exception. Within the *Crocidura poensis* species complex, six species are currently described and recognized in West Africa, but a recent study suggested the existence of an additional cryptic species based on dorsal skull morphology. Here, an integrative approach combining the complete mitochondrial genome, eight nuclear markers, external morphology and geometric morphometrics methods on the skull and mandible of the *C. poensis* species complex distributed across West Africa is used to test the validity of the new candidate species. Species delimitation analyses performed separately on nuclear and mitochondrial DNA support the existence of seven species. Despite low genetic distance with its closest relative, the new species can be distinguished by several diagnostic nucleotide characters using cytochrome b sequences, by morphometric analyses on the skull and mandible as well as traditional external measurements. This allowed us to describe the new species as *Crocidura pediculus* Voet, Cornette & Nicolas sp. nov.

Keywords. Geometric morphometrics, species delimitation, species description, systematics, West Africa.

Voet I., Delapré A., Denys C., Lalis A., Cornette R. & Nicolas V. 2026. Integrative taxonomy resolves a new West African *Crocidura* (Mammalia: Soricidae) species, cryptic to *Crocidura grandiceps* in color, but distinct in size. *European Journal of Taxonomy* 1039: 297–322. https//doi.org/10.5852/ejt.2026.1039.3197

Introduction

The West Africa (WA) subregion is the area delimited by the outermost borders of Mauritania, Mali, Niger and Nigeria, comprising the countries in the southern half of the western part of Africa (CILSS 2016). It is home to a wide range of climates and landscapes, bounded by the Sahara to the north, the Atlantic Ocean to the South and West, and by the Cameroon volcanic line to the East. Although the landscape is overall flat and of low elevation, mostly between 0 and 1000 m a.s.l., the surrounding desert and ocean create variable conditions responsible for the diverse climate and vegetation in WA. Based on long-term annual rainfall, five bioclimatic regions have been defined in WA, from dry to wet: The Saharan, the Sahelian, the Sudanian, the Guinean and the Congo-Guinean. Each of these regions is home to different vegetational types, from desert and savannas to dense tropical forests. Due to the diverse climate and vegetation, WA records high levels of biodiversity, in particular within the Guinean Forests of the WA hotspot. Since 1960, annual rainfall has slightly decreased, and shifts in the bioclimatic region boundaries have been detected, highlighting the sensitivity of the vegetation types to climate change (Heubes *et al*. 2011). During the Pleistocene, climatic shifts occurred on longer time scales and with higher intensity, repeatedly changing the vegetation patterns in WA (deMenocal 2004; Trauth *et al*. 2009). Periods of colder and dryer climate lead to the retreat of tropical forests into fragmented patches, leading to the isolation of habitat-specific populations and the creation of highly heterogeneous landscapes. This climatic and vegetational instability, in addition to the presence of many river basins, is believed to have led to the high levels of species diversity and endemism observed in WA. Small mammals in particular may have been more sensitive to these events, with their rapid generation time and fast evolution (Jacquet *et al*. 2014; Bohoussou *et al*. 2015; Hassanin *et al*. 2015). Other speciation modes have been proposed in this subregion such as ecological speciation resulting from environmental gradients (Nosil 2012; Zhen *et al*. 2017).

Whether the result of geographic isolation or environmental gradients, high species richness in tropical WA has been demonstrated for many species groups, among which shrews (Eulipotyphla, Soricidae) are no exception (Hutterer & Happold 1983; Churchfield *et al*. 2004; Jacquet *et al*. 2012; Nicolas *et al*. 2020; Amori *et al*. 2021; Denys *et al*. 2021; Mamba *et al*. 2021). Among shrews, the genus *Crocidura* Wagler, 1832 is particularly species-rich, representing the mammal genus with the highest number of known species (Wilson & Mittermeier 2018). The exact count is yet to be determined, due to their conservative morphology, uneven sampling, unstudied lifestyles and lack of or confusing genetic data (Voet *et al*. 2022). Over 210 species are listed throughout the world in the most recent checklists, and more are discovered on a yearly basis using integrative approaches (Ceríaco *et al*. 2015; Konečný et al. 2020; Esselstyn *et al*. 2021; Craig *et al*. 2025), either from newly collected individuals or from the rigorous combination of the study of genetic markers and use of geometric morphometric methods on museum specimens. When species determination is uncertain due to overly similar morphologies and the insufficiency of traditional identification methods, species are often grouped within species complexes and referred to as cryptic species (Fišer *et al*. 2018). Many such complexes exist within the genus *Crocidura*, such as the *C. poensis* Fraser, 1843 species complex (Nicolas *et al*. 2019). This species complex has one of the highest species counts, with ten currently identified lineages, distributed across tropical Africa (Nicolas *et al*. 2019; Konečný *et al*. 2020). Out of these ten genetically confirmed lineages, the six found in WA form a monophyletic group and five of those are highly overlapping in their geographic distributions. The allopatric exception, *C. foxi* Dollman, 1915, has been captured in Benin, Ghana, Cameroon and Nigeria, occurring east of the Dahomey Gap. *Crocidura* cf. *longipes*, temporarily named as such in Nicolas *et al*. (2019) based on *C. longipes* Hutterer & Happold, 1983, is present the furthest to the west, in Senegal and Guinea; *C. theresae* Heim de Balsac, 1968 is found from Guinea to Burkina Faso, *C. buettikoferi* Jentink, 1888 and *C. grandiceps* Hutterer, 1983 were captured in Guinea, Ivory Coast, Liberia and Ghana; lastly, *C. wimmeri* Heim de Balsac & Aellen, 1958 is found in Ivory Coast and Ghana. Following the publication of the phylogeny of the *C. poensis* species complex (Nicolas

et al. 2019), a study investigating the morphology of the species within the complex found higher morphological disparity in *C. grandiceps*, as high as twice the value found within the other species (Voet *et al*. 2022). The morphospace showed two near distinct convex hulls, unusual phenomenon within a single species. Moreover, mitochondrial DNA markers displayed two distinct monophyletic clades within this species with high support values, leading to the hypothesis of an additional candidate species, *C.* cf. *grandiceps*. A candidate species being a population with sufficient evidence for its recognition as a species, but having not yet been formally described (Padial *et al*. 2010). In Voet *et al*. (2022), the species *C. grandiceps* was temporarily split in two lineages, *C. grandiceps* and *C.* cf. *grandiceps*, awaiting a more complete diagnosis and formal description.

In this paper, an integrative approach was used to clarify the taxonomy of *C. grandiceps*. With the complete mitochondrial genome and eight nuclear markers, molecular phylogenies were reconstructed for the WA species of the *C. poensis* species complex, and species delimitation approaches were used to test the *C.* cf. *grandiceps* species hypothesis. In addition, external morphology as well as skull and mandible size and shape of the geographically WA overlapping species of the *C. poensis* species complex were investigated using geometric morphometric methods. BPP species delimitation analyses performed separately on nuclear and mitochondrial DNA support the existence of seven species. Despite low genetic distance with its closest relative, the new species can be distinguished by several diagnostic nucleotide characters using cytochrome b sequences, by morphometric analyses on the skull and mandible as well as by traditional external measurements. This allowed us to validate and describe the new species.

Material and methods

Sampling

As mitochondrial lineages can be used to determine which species a specimen can be attributed to in the *C. poensis* species complex (Nicolas *et al*. 2019), cytochrome b (Cytb) and 16S sequences were collected from GenBank or newly produced. Taking into consideration the West African clade's monophyly and geographic segregation, the focus was set on those species instead of the complete *C. poensis* species complex. The Cytb and/or 16S sequences of between seven and 277 individuals per species or candidate species were gathered (for a total of 443 specimens). Among those, 37 were successfully sequenced for the complete mitogenome (*C. theresae*, 10; *C.* cf. *grandiceps*, 6; *C. grandiceps*, 2; *C.* cf. *longipes*, 5; *C. buettikoferi*, 6; *C. wimmeri*, 1; *C. foxi*, 7) along with eight nuclear markers (36 successful, 1 *C. buettikoferi* fewer). The skulls and mandibles of genetically identified individuals were also used to quantify the morphological variation between species and candidate species. A total of 98 specimens in dorsal view, 94 in ventral view and 85 mandibles were examined, for a total of 85 individuals with all three intact structures. External body measurements of up to 414 of the 443 genetically identified specimens were examined as well.

Genetics

Sequencing and assembly

Rapid approximate-maximum-likelihood (approximate-ML) trees were reconstructed for multiple Cytb and 16S datasets of variable sequence length depending on individual coverage using FastTree (Price *et al.* 2010) and the CAT-GTR model. The reliability of nodes was calculated using local support values like in PhyML3. These trees were used as a base for the assignment of specimens to mitochondrial lineages, to use as a reference for the morphometrics analyses. The choice of outgroups was based on the paper on shrew diversity by Dubey *et al.* (2008), and the availability of their sequences on GenBank. The twelve species used can be found in SM1.

From the complete dataset, a subset containing a total of 404 complete Cytb sequences were extracted for the six recognized species present in WA (*C.* cf. *longipes*, *C. buettikoferi*, *C. grandiceps*, *C. theresae*, *C. wimmeri* and *C. foxi*) and the candidate species *C.* cf. *grandiceps*. This complete Cytb dataset was used to construct the approximate-ML tree (Fig. 1). Using that tree and the other rapid approximate-ML trees (from partial sequences) as a baseline, individuals were selected based on clade and locality for the further sequencing of the complete mitochondrial genome and eight nuclear markers. In individual-rich clades, conspecific specimens were preferentially chosen from different localities, in an attempt to optimize geographic sampling and obtain a good representation of genetic variability. They were also preferentially selected from complete Cytb sequences of excellent quality to maximize the likelihood of successful further sequencing, assuming that these samples had good DNA quality. The complete mitochondrial genome (apart from the control region) was obtained by long-range PCR of three overlapping fragments using LongAmp Taq DNA polymerase (New England BioLabs Inc., Ipswich, MA) and sequenced using the Illumina sequencer of the "Service de Systématique Moléculaire" of the MNHN. The reads were loaded into Geneious Prime 2021.1.1 (https://www.geneious.com/) (Kearse *et al*. 2012), trimmed by an error probability algorithm and mapped to a *Crocidura buettikoferi* reference mitogenome (GenBank no. PX633553.1), with a maximum mismatch of 3%. Primers were mapped onto the consensus

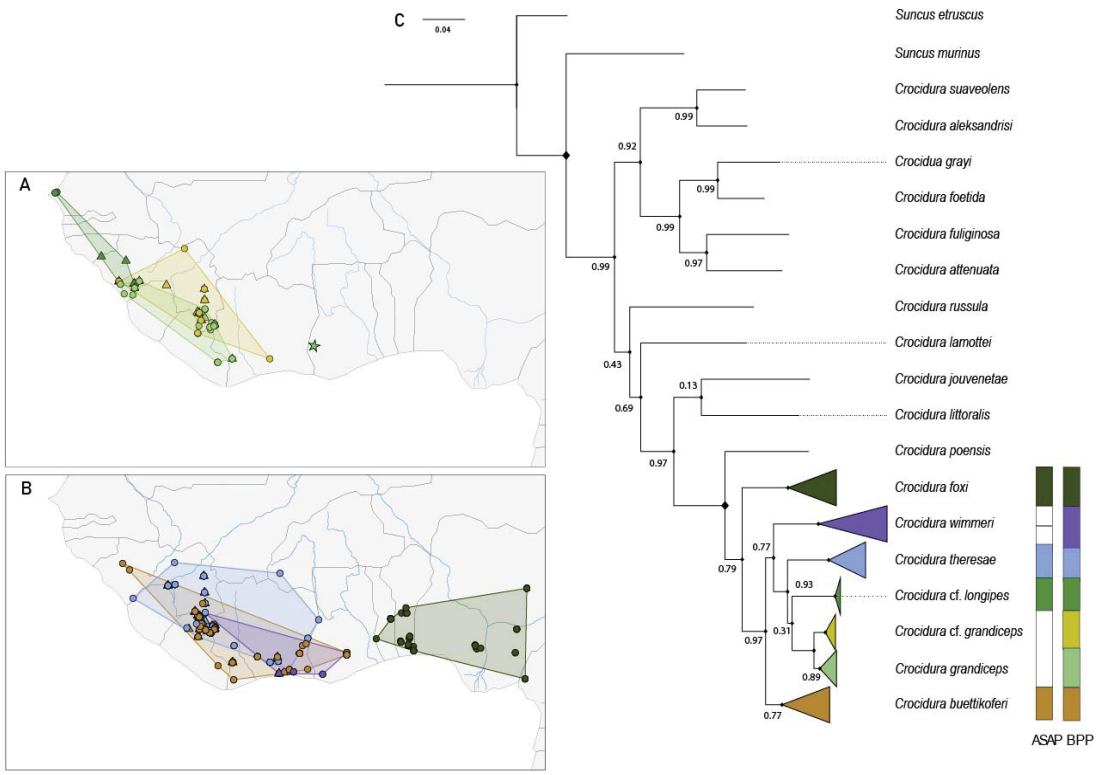

Fig. 1. Maps of all specimens with available Cytb and/or 16S sequences and approximate -maximum-likelihood tree of complete Cytb sequences. Inclusion in the morphometrics analyses is shown by shape (circles indicate specimens without morphometrics data and triangle specimens with both morphometrics and genetic data). The *C. grandiceps* Hutterer, 1983 holotype was included in the morphometrics study and is shown by a green star. **A**. Map of *Crocidura grandiceps*, *C.* cf. *grandiceps* and *C.* cf. *longipes*. **B**. Map of *C. theresae*, *C. wimmeri*, *C. buettikoferi* and *C. foxi*. **C**. On the tree, node support values of 1 are shown by large diamonds. Colored boxes on the right side indicate the best ASAP partition and the species supported by the BPP analysis for 7 candidate species.

sequence and reads anteriorly located to the primer were removed. Sequences were aligned using the MAFFT plugin (ver. 7.450) on Geneious Prime and default settings. Alignments were visually checked for errors and excessive gaps, and manually corrected. From the complete mitochondrial genome, 12 coding genes and the non-coding RNA fragments (16S and 12S, ribosomal RNA and all transfer RNA) were extracted individually and reassembled by grouping the coding genes and concatenating all non-coding fragments terminally. Coding gene alignments were verified by translation into protein sequences. For 36 individuals, eight nuclear genes were amplified by short-range PCR and sequenced using the Illumina sequencer. Eight nuclear markers were selected based on previous works: the five exons ApoB, BDNF, BRCA1, GHR and vWF, and the three introns HDAC2, MCGF and STAT5A. All primers for the mitochondrial fragments and the nuclear genes can be found in SM2 Table 1, as well as complete gene names and intron/exon fragments.

Phylogenetic tree reconstructions

Our final dataset comprised 37 ingroup individuals with complete or near-complete mitogenomes and 36 with nearly all of the eight selected nuclear markers. The mitogenome dataset comprised 14 743 positions with 3.3% of missing data. The nuclear dataset had 4597 positions with 11.1% of missing data (missing positions in the concatenated dataset) and 12.5% of missing loci. Eleven of the twelve outgroups chosen for the Cytb and 16S approximate-ML trees were used for the complete mitogenome, nine were used for the nuclear dataset. For the mitogenome, we tested 39 partitions: the 12 coding genes separated by codon position, the two ribosomal subunits, and all tRNAs put end-to-end, the sequences being too short to carry information in individual analyses. The nuclear dataset was partitioned using the same principle. All exons (ApoB, BDNF, BRCA1, GHR and vWF) were partitioned by codon position. The three introns (HDAC2, MCGF1, and STAT5A) were examined individually but without codon position partitioning. For both datasets, all models from MrBayes were tested with linked branch lengths and the greedy algorithm, and the best partitions and models were selected using the Bayesian information criterion (BIC). Maximum likelihood (ML) trees were reconstructed using the IQ-TREE Web Server (http://iqtree.cibiv.univie.ac.at) (Nguyen *et al*. 2015). Providing a specified partition and sequence alignment, IQ-TREE simultaneously outputS the best partition scheme, models and consensus tree. Linked branch lengths was selected and node support was calculated through ultrafast bootstrap ping with 1000 replicates (Hoang *et al*. 2018). Before running the Bayesian reconstructions, as MrBayes does not simultaneously calculate the best partition, PartitionFinder2 ver. 2.1.1. (Lanfear *et al*. 2017) was used to detect the best schemes and substitution models. The best schemes were then used in the Bayesian tree reconstructions with MrBayes ver. 3.2.7a (Ronquist & Huelsenbeck 2003). For each dataset, two independent runs of four chains (MCMC) were run for 5 000 000 generations and sampled every 100 generations, checking convergence with Tracer ver. 1.7.2 (Rambaut *et al*. 2018) and discarding the first 25% as burn-in.

Sequence divergence and species delimitation

Cytb divergence between species was calculated using the K2P model on MEGA ver. 7.0.26 (Kumar *et al.* 2016), over 404 complete Cytb sequences. The K2P model was used in order to compare values with other species groups, while being aware that it may not be appropriate for closely related species (Srivathsan & Meier 2012). Two methods were used to test our species delimitations. 1) Assemble species by automatic partitioning (ASAP is available through the spart explorer website: https://spartexplorer.mnhn.fr/) (Puillandre *et al.* 2021) which is a prior-free method that requires only a sequence alignment to estimate species partitions was used. This method uses a hierarchical clustering algorithm, generating potential species partitions depending on between-group genetic distance matrices. As it does not accommodate recombination, it is traditionally used on monolocus alignments (mitochondrial barcodes such as Cytb or COI). Prior-free partitions were tested in our complete Cytb dataset (outgroups excluded) as well as in the complete mitogenome dataset. Both the Jukes-Cantor

and the Simple Distance (*p*-distance) methods were tested. The K2P model was excluded for the reason specified above (Srivathsan & Meier 2012). 2) Bayesian Phylogenetics and Phylogeography (BPP ver. 4.6.1) (Yang 2015) was used to jointly estimate the species delimitations and species trees (A11 analysis). BPP uses the multispecies coalescent model (MSC) (Rannala & Yang 2003; Jiao *et al.* 2021) and gene sequence alignments in a Bayesian Markov chain Monte Carlo program to assign posterior probability values to predefined species hypotheses and output a sample of posterior species trees. Three datasets were used (without outgroups): the complete Cytb set, the complete mitochondrial DNA set, and the gene-partitioned nuclear dataset, with as candidate lineages the six WA species found in Nicolas *et al*. (2019) and the candidate species *C.* cf. *grandiceps*. Since for the nuclear data, the sequences are polymorphic and unphased, the phasing option was switched on. BPP requires two priors: root divergence time (t_0) and population size (qs). Both were calculated empirically using our three datasets, and set to inverse gamma priors. The parameter t_0 was calculated using the maximum observed genetic difference divided by two which for the nuclear dataset gave an inverse gamma distribution of a = 3 and b = 0.0035. For qs, we used a = 3 and b = 0.006, corresponding to the average distance between individuals from the same lineage. The priors were calculated individually for each dataset. The starting tree used was the species tree obtained in Voet *et al.* (2022) and cropped to include only the species of interest. The Cytb analyses were run five times independently with random seed numbers, 10 000 000 iterations and a burn-in of 20%. For the mitochondrial DNA, we changed the number of iterations to 5 000 000, and for the nuclear DNA, we kept the value of 10 000 000, as a compromise between number of specimens and number of sites, using preliminary test runs to verify convergence. Outputs of the BPP analyses were imported into R (R Core Team 2021) and converted into files readable by FigTree and Tracer (https://github.com/onmikula/bpptools). Convergence of runs was verified using Tracer. The maximum clade credibility tree was extracted from the posterior species trees sample using the mean common ancestry node heights, and compared across runs. Species candidates and their average posterior probabilities are shown at the tips, and average posterior probabilities of nodes are displayed on the same tree. The average was calculated over the five independent runs for each dataset.

Diagnostic Cytb nucleotides

To identify diagnostic nucleotide characters for the new candidate species we used MOLD software (Fedosov *et al*. 2022) based on the Cytb alignment used for the phylogenetic analysis. Unlike traditional approaches that identify Diagnostic Nucleotide Characters (DNCs) based solely on observed sequence differences, MOLD employs a robust procedure of iterated haplotype subsampling in order to simulate the impact of unsampled intraspecific genetic diversity and therefore, the genetic variation likely present in nature but absent from the dataset due to limited sampling. Only those sites that consistently retain their diagnostic power across multiple resampling replicates are retained as redundant Diagnostic Nucleotide Characters (rDNCs) as they are considered more robust descriptors of a taxon: less sensitive to sampling artifacts and more likely to remain valid as additional genetic data become available.

Morphology

Using Cytb and 16S sequences for lineage identification, individuals of interest were selected as such: within the geographically overlapping WA species (all except *C. foxi*, wich is allopatrically distributed to the east of the Dahomey Gap), study specimens were selected based on skull and mandible integrity, age group (SM2 Fig. 1), and geographic location (SM1), aiming for intact adults and good geographic coverage within the species. A geometric morphometrics approach was used to investigate skull and mandible form (i.e., size and shape) (Needham & Hardy 1950; Cooke & Terhune 2015). The structures were photographed by a single person using a NIKON 5600 camera with a 60 mm AF-S Micro NIKKOR lens. The tpsDIG2 ver. 2.31 software (Rohlf 2005) was used to place 28 and 78 landmarks on the dorsal and ventral faces of the skull. For the mandible, a combination of 15 anatomical landmarks and 80 sliding semilandmarks (Bookstein 1991) were digitized. The landmark placements and their descriptions

can be found in SM2 (Fig. 2, Table 2). Sliding semilandmarks were added to the mandibular body and coronoid process to compensate for the absence or rarity of homologous landmarks on important functional structures (Cornette *et al*. 2015a; 2015b). The final datasets comprised 98 specimens in dorsal view, 94 in ventral view and 85 mandibles, for a total of 85 specimens with all three intact structures. The type specimen of *C. grandiceps* was landmarked as well. Landmark files were imported into R, and all subsequent operations were conducted using the *geomorph* and *Morpho* R packages (Adams & Otárola-Castillo 2013; Schlager *et al.* 2020). Differences in position, rotation and scale were removed using Generalized Procrustes Analyses (Rohlf & Slice 1990). On the mandible, the sliding semilandmarks were allowed to glide along the average curve while minimizing bending energy (Gunz & Mitteroecker 2013). For the skulls (bilaterally symmetrical structures), the aligned coordinates were then corrected for asymmetry. Initial individual selection had been done based on age, preferentially landmarking adult specimens. However, for some species in which fewer skulls were readily available, younger individuals had to be included to increase sample size. ANOVAs and MANOVAs were run on all three structures in order to test whether age had a significant effect on size and shape, and whether an interaction existed between species and age. Sexual dimorphism in size and shape was also tested. Principal Component Analyses (PCA) were run separately on all three structures (including the type) and the corresponding morphospaces were displayed with the deformations along the axes in order to quantify and visualize shape differences. Shape averages for each species and structure were plotted against the general average with a magnification factor of five. Canonical Variates Analysis (CVA) was run on all three structures, and displayed with the deformations along the axes. Using mitochondrial lineages as the species grouping variable, CVA was used to maximize between group differences and help in the discovery of diagnostic anatomical structures in species identification. The CVA was run on the PCs capturing 90% of shape variability, on a dataset excluding the type specimen of *C. grandiceps*. Pairwise comparisons were made between species on all three structures with a Tukey test with Bonferroni correction for size, and the distribution of pairwise statistics for shape (Collyer & Adams 2021). Pairwise comparisons were also performed on traditional external body measurements to test for significant differences between species. *Crocidura wimmeri* was excluded from the comparisons as only one specimen was available. In addition, alcohol-preserved specimens were dried and observed for outward appearance and color differences.

All specimens used in the genetic and morphometric analyses and their information can be found in SM1.

Results

Genetics

Both the ML and Bayesian mitogenome trees (Fig. 2) are very well resolved, with all nodes displaying posterior probabilities of 0.99 or more for the Bayesian analysis, and bootstrap support values of over 83 for the ML analysis. All six WA species confirmed in Nicolas *et al*. (2019) are recovered, with the newly identified *C.* cf. *grandiceps* forming a monophyletic clade, a sister species to *C. grandiceps*. The *C. grandiceps* – *C.* cf. *grandiceps* clade is a sister to *C.* cf. *longipes*. These three clades have overlapping distributions in Guinea and Liberia.

The nuclear tree displays the same results as in Nicolas *et al*. (2019), with lower support values than in the mitochondrial DNA and *C. buettikoferi* appearing as a paraphyletic clade (Fig. 3). The species *C.* cf. *longipes, C. grandiceps* and *C.* cf. *grandiceps* appear as a single group.

Cytb genetic distances are presented in SM2 Table 3. *C.* cf. *grandiceps* displays 2.6% genetic distance with *C. grandiceps*, and 6.2% with *C.* cf. *longipes*, its two closest relatives. All other pair comparisons output values between 6.7 and 13.6%. The best partition in ASAP for the complete Cytb sequences retrieves seven species, grouping *C. grandiceps* and *C.* cf. *grandiceps* in one clade (Fig. 1). The four sequences of *C. wimmeri* are split in two lineages, separating the specimens from Ghana and Ivory Coast.

The complete mitogenome dataset returns nine lineages in the best partition (Fig. 2), this time separating *C. grandiceps* and *C.* cf. *grandiceps*. This partition also isolates two specimens (one *C. theresae* and one *C. buettikoferi*) from their respective species. However, at least for specimen BH45 (*C. theresae*), this placement is likely an artefact caused by the high proportion of missing data (25%) in its sequence.

The species delimitation performed with BPP on the Cytb sequences outputs higher posterior probabilities for the seven species hypothesis (Fig. 1). All the candidate species are supported with posterior probabilities of 1 for Cytb (SM2 Fig. 3). For the complete mitochondrial DNA, the five independent runs support the seven species hypothesis with an average posterior probability ranging

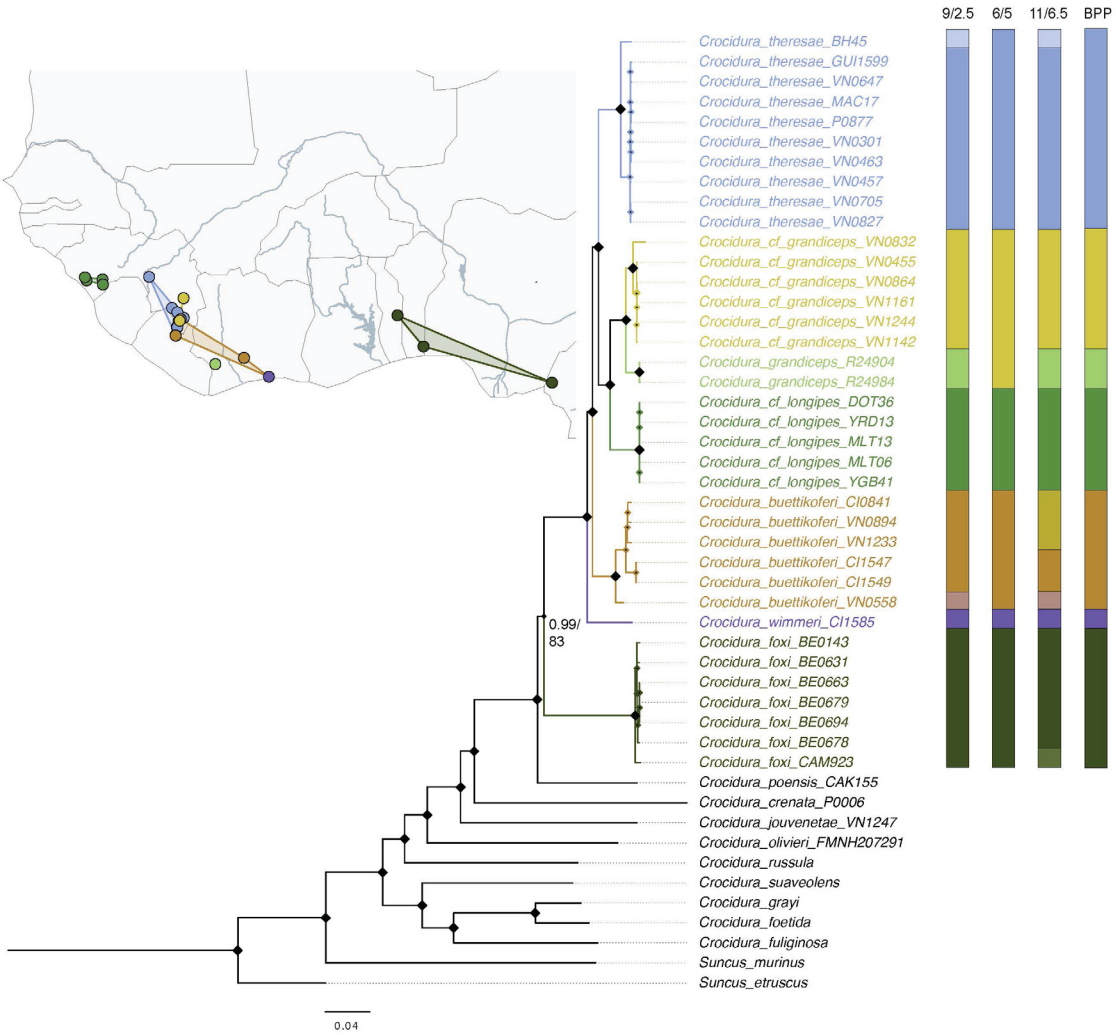

Fig. 2. Map of sampled specimens and Bayesian tree of the complete mitochondrial genome reconstructed using MrBayes. Posterior probabilities (Bayesian) and bootstrap values (ML) are shown on nodes (PP/BS). Clade nodes with support values of 1 (PP) and 100 (Bootstrap) are displayed by large black diamonds. Within species, support values are not shown for clarity. Colored boxes on the right correspond to the three best species partitions produced by ASAP, sorted by ASAP score (lowest score = best partition), and to the species supported by BPP analyses for seven candidate species. Numbers above the colored boxes indicate the number of species partitions obtained and the ASAP score.

between 0.87 and 1.00 (SM2 Fig. 3). The reconstructed BPP tree is the same as the ML and Bayesian trees, although the nodes have low support values. The BPP species delimitation performed on the eight independent nuclear markers supports the existence of the seven WA species in all five independent runs, with posterior probabilities of 1 for each species. *Crocidura cf. grandiceps* emerges as the closest relative to *C.* cf. *longipes*, even if the posterior probability is relatively low (0.92; Fig. 3).

MOLD analysis reveals four nucleotides on the Cytb gene that are shared by all members of *C.* cf. *grandiceps* and by no member of the reference taxa: sites 201: 'A', 579: 'G', 783: 'T' and 1071: 'A'. However, only three of them are considered as reliable diagnostic nucleotide characters by the software: 'A' in the site 201, 'G' in the site 579, 'T' in the site 783.

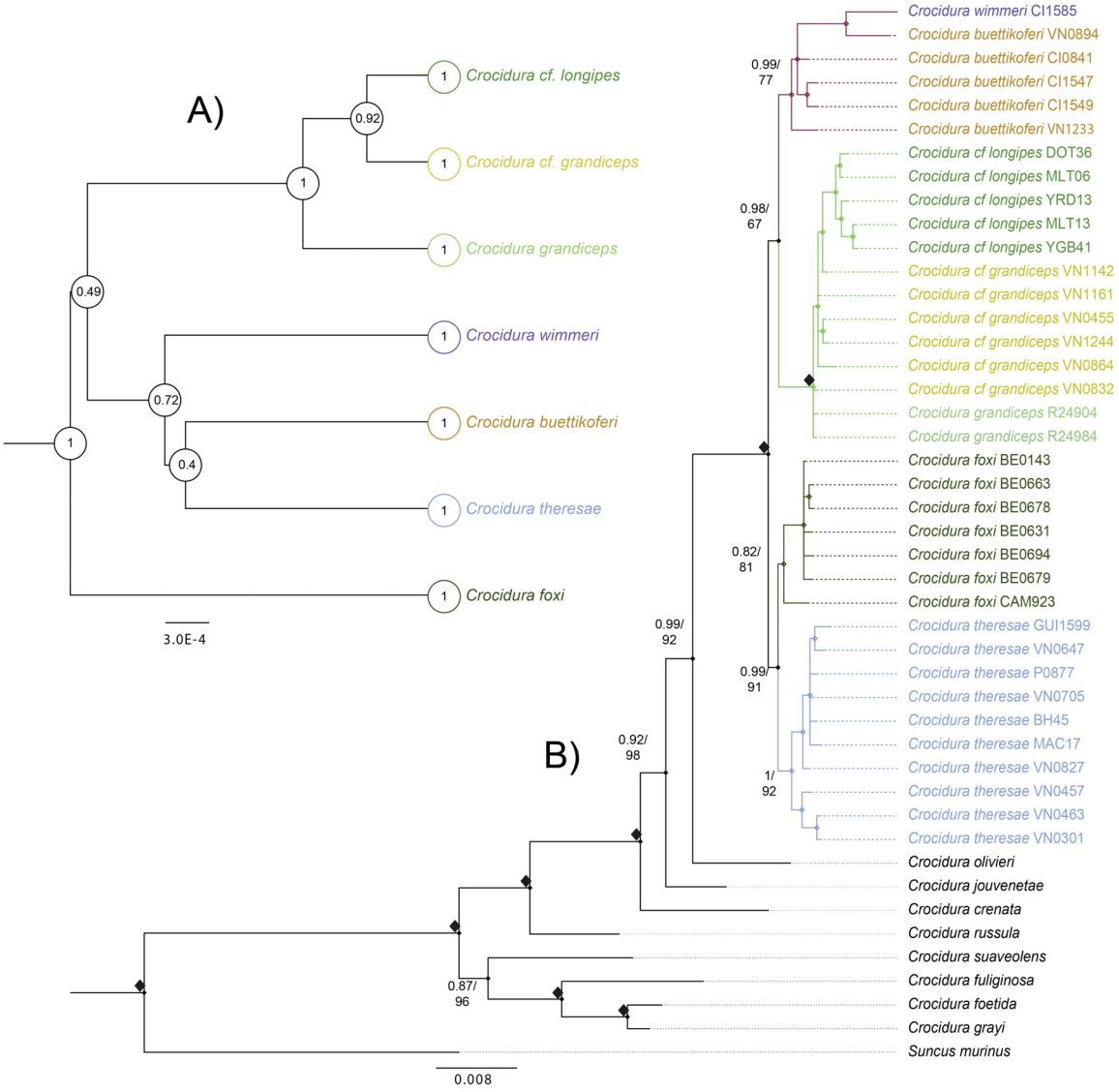

Fig. 3. A. BPP nuclear species tree. Posterior probabilities for species and nodes are shown on the tree. **B.** Bayesian tree of the concatenated nuclear dataset reconstructed using MrBayes. Posterior probabilities (Bayesian) and bootstrap values (ML) are shown on nodes (PP/BS). Clade nodes with a support value of 1 are displayed as large black diamonds. Intraspecific clade node support values are not shown for clarity.

Morphology

In all three bone structures (skull in dorsal and ventral view and mandible), the age and species variables have a significant effect on size and shape, but no interaction could be detected between them (SM2 Table 4). Likewise, the test for sexual dimorphism on size and shape outputs non-significant results. As a result, all specimens were kept as a pooled sample. Size boxplots (Fig. 4) display the log-transformed centroid size for the three structures. In dorsal view, from smallest to largest, the order is as such: *C. theresae, C.* cf. *grandiceps, C. buettikoferi, C.* cf. *longipes* and *C. grandiceps*. However, the mandibule of *C.* cf. *grandiceps* appears to be smaller than that of *C. theresae*. Pairwise size comparisons (SM2 Table 5) show that for all three structures *C.* cf. *grandiceps* can only be discriminated from *C. grandiceps*. *Crocidura grandiceps* is the only species that differs in size from all others. *Crocidura buettikoferi*, the second largest species in our dataset, differs in size from *C. theresae*, the smallest species. Pairwise shape comparisons (Table 1) result in significant differences being observed in nearly all pairs apart from *C.* cf. *grandiceps* – *C. theresae.* Among the three closely related *C. grandiceps*, *C.* cf. *grandiceps* and *C.* cf. *longipes*, *C.* cf. *grandiceps* is significantly different from *C.* cf. *longipes* only in the dorsal view (d = 0.02, Z = 1.81, p = 0.034*), and from *C. grandiceps* in the dorsal and ventral views of the skull (d = 0.029, Z = 4.560, p = 0.001* and d = 0.030, Z = 4.006, p = 0.001*, respectively), but not the mandible. The

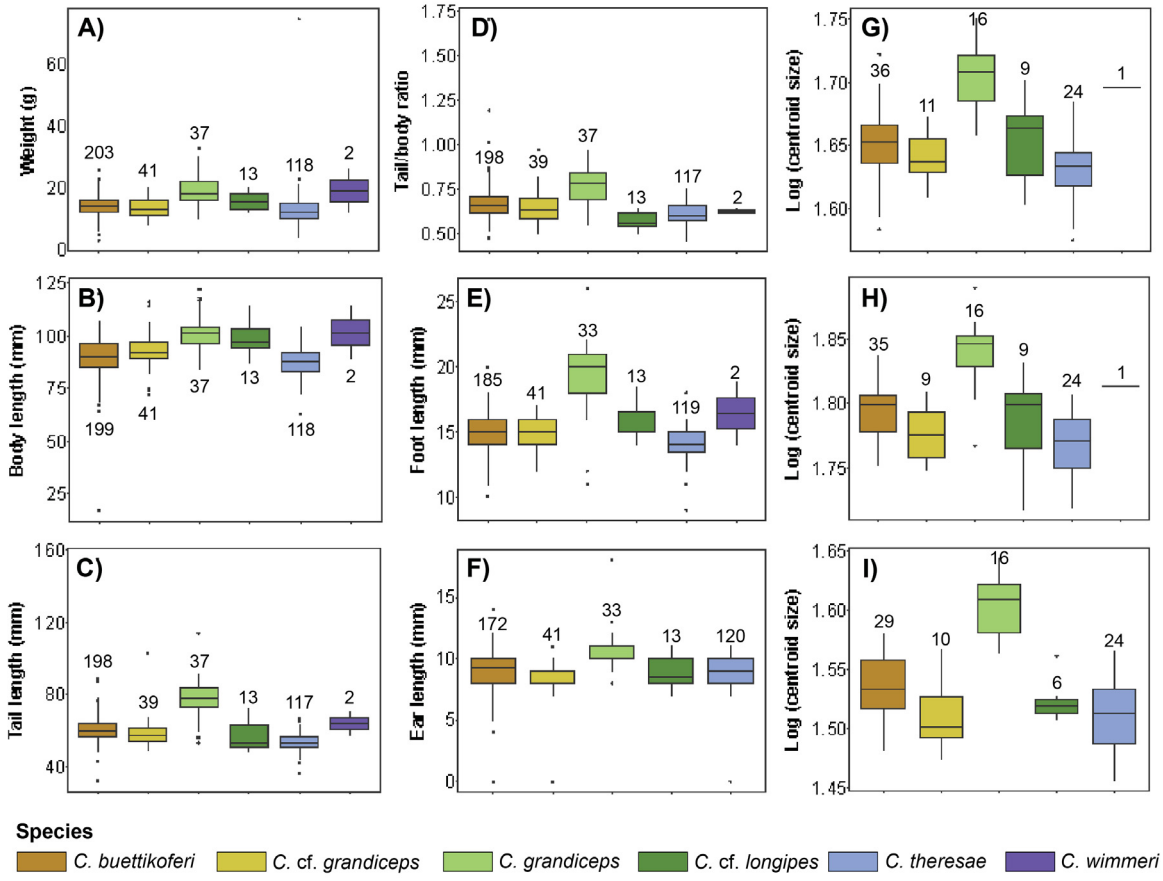

Fig. 4. Size boxplots. Sample sizes are displayed for each species above the corresponding box. **A**.Weight. **B**. Body length. **C**. Tail length. **D**. Tail/body ratio. **E**. Foot length. **F**. Ear length. **G**. Log centroid sizes of the skull in dorsal view. **H**. Skull in ventral view. **I**. Mandible.

Table 1. Pairwise comparisons (distribution of pairwise statistics) of shape of the skull in dorsal view, the skull in ventral view and the mandible. Significance is marked by asterisks and d is the mean distance between species. Bold pairs are species with at least two significant differences.

	Skull dorsal			**Skull ventral**			**Mandible**		
	d	**Z**	**Pr(>d)**	**d**	**Z**	**Pr(>d)**	**d**	**Z**	**Pr(>d)**
C. buettikoferi* – *C. cf. grandiceps	0.014	2.274	0.015*	0.018	2.893	0.003*	0.019	1.510	0.062
C. buettikoferi* – *C grandiceps	0.022	4.605	0.001*	0.021	4.199	0.001*	0.022	2.548	0.005*
C. buettikoferi* – *C cf. longipes	0.022	4.254	0.001*	0.025	3.841	0.001*	0.021	0.986	0.146
C. buettikoferi* – *C. theresae	0.015	3.618	0.001*	0.012	2.846	0.001*	0.018	2.383	0.009*
C. cf. grandiceps* – *C. grandiceps	0.029	4.560	0.001*	0.030	4.006	0.001*	0.025	2.106	0.022
C. cf. *grandiceps* – *C.* cf. *longipes*	0.017	1.807	0.034*	0.015	1.457	0.074	0.021	0.488	0.314
C. cf. *grandiceps* – *C. theresae*	0.011	1.006	0.146	0.011	0.916	0.179	0.020	1.419	0.073
C. grandiceps* – *C. cf. longipes	0.031	4.945	0.001*	0.033	4.091	0.001*	0.022	0.914	0.170
C. grandiceps* – *C. theresae	0.030	5.329	0.001*	0.028	4.760	0.001*	0.032	4.028	0.001*
C. cf. longipes* – *C. theresae	0.020	3.163	0.002*	0.019	3.083	0.002*	0.023	1.258	0.098

mandible is the least easily discriminated in pair comparisons, with only three significantly different pairs (*C. buettikoferi – C. grandiceps*, *C. buettikoferi – C. theresae* and *C. grandiceps – C. theresae*). Among the other geographically overlapping WA species, *C.* cf. *grandiceps* differs from *C. buettikoferi* in the skull in dorsal and ventral views.

The PCA displays areas of overlap among all species (Fig. 5). The results of the pairwise comparisons are visually concurring with the morphospace, *C. grandiceps* being the most easily discriminated in the skull in dorsal and ventral views, different from the other species primarily along axis 1. *Crocidura* cf. *grandiceps* is largely overlapping with *C. theresae* in both dorsal and ventral skull views, as the absence of significant differences in shape indicated. The overlap is slightly less pronounced between the pair in ventral view, and even less so in the mandible, where the area occupied by *C.* cf. *grandiceps* extends into the morphospace of *C.* cf. *longipes* and *C. grandiceps*. The holotype of *C. grandiceps* falls unambiguously within *C. grandiceps'* convex hull in the dorsal skull view, just outside the convex hull in ventral view, but still closer to *C. grandiceps* than any of the other species, and near the center of the morphospace for the mandible, inside the areas occupied by all other species as well.

In dorsal view, Principal Component 1 (PC1; 26.74% of total shape variability) is mainly represented by differences in the rostrum to braincase size ratio. Negative values are associated with a larger maxillary bone compared to the braincase, as is apparent in *C. grandiceps*. The incisors extend further out anteriorly, the interorbital space is narrower, the articular facets are smaller, and the widest point of

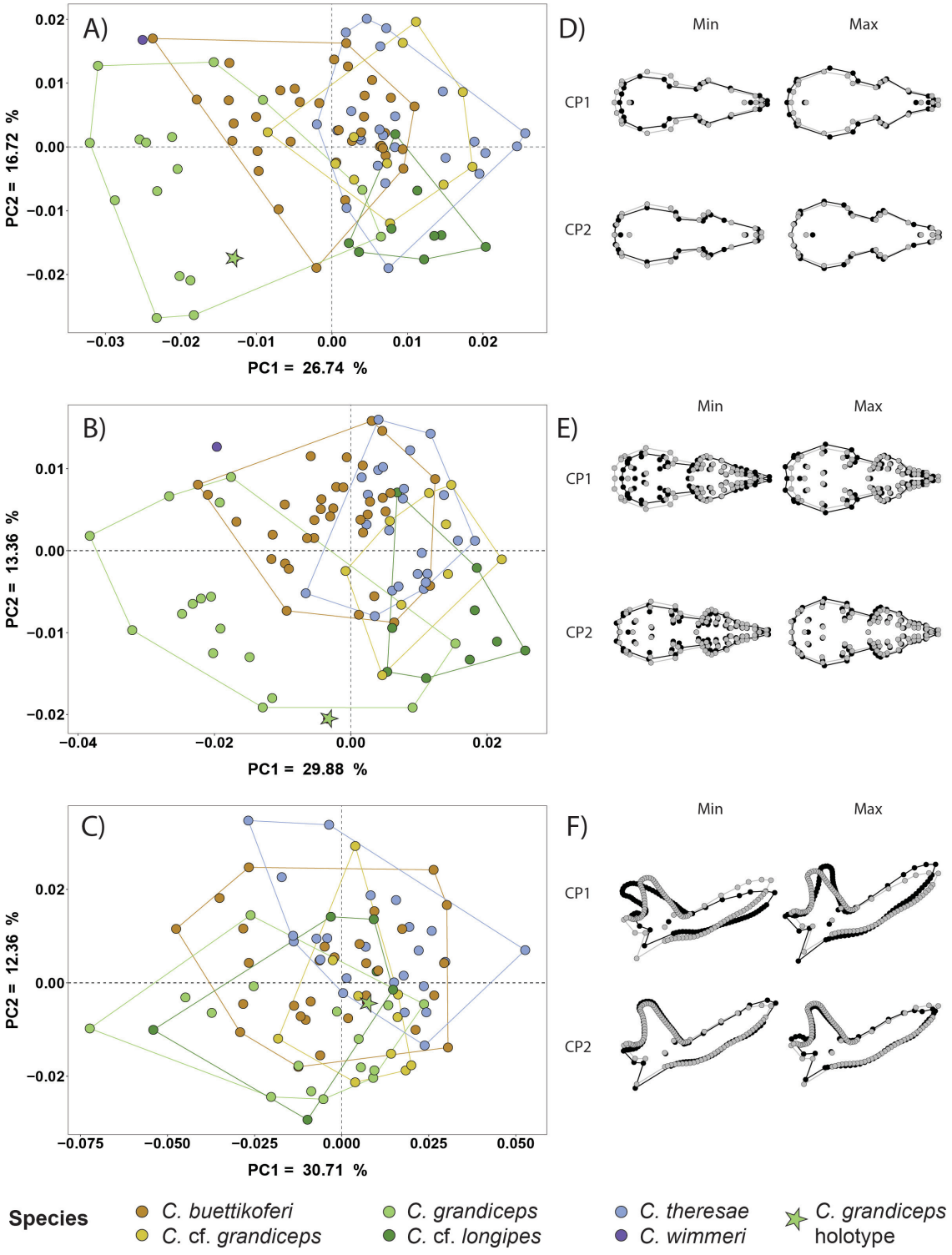

Fig. 5. PCA and deformations. **A-C**. PCA of the aligned coordinates: skull in dorsal view (A), skull in ventral view (B), mandible (C). Species are represented by color. The holotype of *C. grandiceps* Hutterer, 1983 (light green) is shown in the morphospace of all three structures. **D-F**. Deformations along the axes are represented to the right of their respecive PCA plots, with a magnification factor of three. Species are represented by color.

the braincase is more posteriorly located. PC2 captures 16.72% of the total shape variability and its main feature lies in braincase width. Negative values are associated with a narrower, elongated skull, a feature visible in *C. grandiceps* and *C.* cf. *longipes*.

In ventral view, the outline changes are the same as in dorsal view, PC1 (29.88% of total shape variability) mainly capturing the variation in rostrum to braincase ratio, and PC2 (13.36%) the change in skull width. In addition to overall skull shape, PC1 is associated with changes in internal structures. Minimal values correspond to incisors extending further laterally, with a wider rostrum. The molar and the palatine bone extend posteriorly, the palatine bone protruding further into the interorbital area. The braincase being reduced in size, the foramen magnum appears more anteriorly located and the space between the foramen lacerum posterius and the tympanic area is reduced. The maximum values display an extension of the occipital condyles, until their tip is no longer aligned with the posterior extremity of the foramen magnum. PC2 minimum values are associated with the same changes observed in dorsal view as well as the anterior extremity of the foramen magnum being more posteriorly located and the occipital condyles extending further to the back of the skull.

In the mandible, a strong overlap appears between all species. PC1 and PC2 capture 30.71% and 12.36% of total shape variability, respectively. PC1 is mainly associated with changes in coronoid process orientation compared to the mandibular body, the negative values corresponding to a more obtuse angle. Negative values are also matched with a shorter mandibular condyle and angular process. PC2 displays two main areas of variability, positive values being associated with a smaller angle between mandibular condyle and coronoid process, and a more vertical insertion of incisor i1, extending anteriorly towards negative values.

The CVA on the PCs capturing 90% of the total shape variability obtained the highest results in classification accuracy for the skull in ventral view (97.85%). The dorsal view was the least successful, with 81.44% of correct classification, preceded closely by the mandible with 82.35%, only slightly better than the dorsal view. The classification results for each species and structure can be viewed in SM2 Table 6. In dorsal view, *C.* cf. *grandiceps* had one of the highest misclassification scores, with 27.27% of specimens sorted in *C. theresae*, and only 54.55% correctly classified as *C.* cf. *grandiceps*. However, in ventral view, 100% were correctly sorted. The mandible was sorted alternatively into *C.* cf. *grandiceps* (80%), *C. buettikoferi* (10%) and *C.* cf. *longipes* (10%). The CVA plots (SM2 Fig. 4) display deformation results similar to the PCA results: in dorsal view, CV1 (47.05%) and CV2 (32.71%) overall display the same shifts in rostrum to braincase ratio and braincase shape, but contrary to CP2, CV2 shows a focus on braincase elongation and lateral curvature. *Crocidura grandiceps* can be distinguished from the other species along axis 1, and axis 2 only partially separates *C. theresae* and *C. buettikoferi* from *C.* cf. *longipes*. In ventral view, CV1 (50.18%) and CV2 (27.13%) display reversed changes compared with the PCA, CV1 capturing differences in braincase shape and elongation, and CV2 those in rostrum – braincase ratio. *Crocidura grandiceps* can be differentiated from *C. buettikoferi* and *C. theresae* along axis 1, and from *C.* cf. *longipes* and *C.* cf. *grandiceps* along axis 2, with no overlap. Likewise, there is no overlap between *C. grandiceps* and *C.* cf. *grandiceps* in dorsal and ventral views. In the mandible, the shifts along the axes are more subtle than in the PCA, and slightly different. The overlap among species is higher than in the other structures. CV1 (72.44%) captures shifts in mandibular body length and coronoid process orientation, and *C. grandiceps* barely stands out along the positive values of CV1. CV2 (17.44%) does not allow any discrimination.

PCA and CVA plots along with the average represented shape of each species (SM2 Fig. 5) highlight several key features in distinguishing the species geographically overlapping in WA. From smallest to largest species, *C. theresae* is characterized by a large braincase, its maximum width placed anteriorly. In the rostrum, the area carrying the incisors is narrower, and that of the molars extends further laterally.

Crocidura cf. *grandiceps* resembles *C. theresae* most closely in the skull, the main difference lying in the width of its maxillary bone, and the placement of the foramen magnum compared with the occipital condyles, closer to *C.* cf. *longipes*, explaining the overlap on the PCA and CVA. The skull of *Crocidura* cf. *longipes* is elongated, the rostrum to braincase remaining small. The interorbital area is more anterior and the braincase extends posteriorly. *Crocidura buettikoferi* lies in the center of the morphospace for all three structures, its shape closely resembling the general average, with a rounded braincase and short rostrum. The largest, *C. grandiceps,* is the most easily discriminated in the skull, with an elongated rostrum and small braincase compared to the whole. The palatine bone extends much further into the interorbital area. In the mandible, two main differences arise on the average shapes: the length of the mandibular body for *C. grandiceps* and the length of the angular process in *C.* cf. *grandiceps*.

The comparison of external body measurements results in several significant differences between species (SM2 Fig. 6). *Crocidura grandiceps* is larger in size and significantly different from *C.* cf. *grandiceps, C. theresae* and *C. buettikoferi* in all recorded external body measurements. *Crocidura* cf. *grandiceps* differs from *C. buettikoferi* only in ear length (smaller ears) and from *C. theresae* in tail and hindfoot length (longer tail and hindfeet), with weak significance for both. No significant differences were found between *C.* cf. *grandiceps* and *C.* cf. *longipes*, in any of the recorded body measurements. Although non-significant, *C.* cf. *grandiceps* is slightly lighter in body weight than *C. theresae*, but with a longer total body size (tail and hindfoot are both slightly longer).

Taxonomic account

Class Mammalia Linnaeus, 1758
Order Eulipotyphla Waddell, Okada & Hasegawa, 1999
Suborder Erinaceota Van Valen, 1967
Superfamily Soricoidea Gill, 1872
Family Soricidae Fischer, 1815
Subfamily Crocidurinae Milne-Edwards, 1872
Genus *Crocidura* Wagler, 1832

Crocidura pediculus Voet, Cornette & Nicolas, sp. nov.
urn:lsid:zoobank.org:act:A8B3B3AF-5D6B-4EE7-A708-620BB961D19F
Figs 6–7

Crocidura cf. *grandiceps* – Voet *et al*., 2022 : figs 2–4, 6.

Diagnosis (see Figs 6–7 and SM2 Figs 5–6)

The Cytb DNA diagnosis for the taxon *C. pediculus* sp. nov. is: ‘A’ in the site 201, ‘G’ in the site 579, ‘T’ in the site 783.

The new species is distinguished from other members of the West African *C. poensis* group by its small size and pelage coloration. It closely resembles *C. grandiceps* in having a dark brown dorsal pelage, a slate-brown belly, and a gradual transition between the two (Fig. 6). The tail is long, dark brown to black, and fully haired. However, *C. pediculus* sp. nov. is significantly smaller than *C. grandiceps* in both external measurements and skull/mandible dimensions (Fig. 7).

Etymology

The specific name is a noun in apposition, stemming from the Latin *pediculus* ‘little foot’. The species is generally smaller and has significantly smaller hindfeet compared to *C. grandiceps* (Latin: ‘large head’), under which name it has until now been exhibited in museum collections.

Type material

Holotype

GUINEA • ♀ adult; Zogota; 7.944° N, 9.105° W; 2 Feb. 2012; V. Nicolas and A. Lalis leg.; lowland forest; GenBank nos. ON603722 (Cytb); MNHN, MNHN-ZM-2013-503.

Paratypes

GUINEA • 1 ♀ adult; Zogota; 7.944° N, 9.105° W. 30 Jan. 2012; V. Nicolas and A. Lalis leg.; lowland forest; GenBank nos: ON620437 (16S), PX633560 (complete mtDNA), PX054761 (ApoB), PX054815 (BDNF), PX054851 (GHR), PX054907 (MCGF); MNHN, MNHN-ZM-2013-501 • 1 ♂ adult; same locality as for holotype; 4 Feb. 2012; V. Nicolas and A. Lalis leg.; lowland forest; GenBank no.: ON603721 (Cytb); MNHN, MNHN-ZM-2013-504 • 1 ♂ adult; Franfina; 9.63° N, 8.94° W; Feb. 2004;

Fig. 6. Specimens of *Crocidura pediculus* sp. nov. Voet, Cornette & Nicolas **a.** holotype, ♀ MNHN-ZM-2013-503 **b.** Paratype, ♀ MNHN-ZM-2013-501 **c.** Paratype, ♂ MNHN-ZM-2020-1895; and *Crocidura grandiceps* **d.** MNHN-ZM-2017-450 **e.** MNHN-ZM-2017-455. Specimens are preserved in alcohol and were dried prior to taking the pictures.

C. Denys and E. Lecompte leg.; GenBank nos: MH806024 (Cytb), MH782818 (16S); MNHN, MNHN-ZM-2013-772 • 1 ♂ adult; Gbetlaya; 9.84° N, 11.04° W; May 2003; E. Fichet-Calvet leg.; GenBank no.: ON620407 (16S); MNHN, MNHN-ZM-2013-763 • 1 ♀; same data as for preceeding; GenBank nos: MH806017 (Cytb), MH782811 (16S); MNHN, MNHN-ZM-2013-764 • 1 ♂ adult; Hermakono; 9.036° N, 8.918° W; 680 m a.s.l.; 8 Aug. 2011; V. Nicolas and A. Lalis leg.; forest; GenBank nos: PX054599 (Cytb), PX633559 (complete mtDNA), PX054760 (ApoB), PX054794 (BRCA1), PX054814 (BDNF), PX054850 (GHR), PX054883 (HDAC2), PX054906 (MCGF), PX054937 (STAT5A), PX054961 (vWF); MNHN, MNHN-ZM-2013-453 • 1 ♀ adult; Hermakono; 9.036° N, 8.918° W; 680 m a.s.l.; 5 May 2011; V. Nicolas and A. Lalis leg.; forest; GenBank nos: MH806039 (Cytb), MH782832 (16S); MNHN, MNHN-ZM-2013-499 • 1 ♀ adult; Ziama forest, Kazaouma; 8.35° N, 9.217° W; 21 Sep. 2003; V. Nicolas and M. Colyn; fallow; GenBank nos: MH806032 (Cytb), MH782826 (16S); MNHN, MNHN-ZM-2020-1891 • 1 ♂ adult; Ziama forest, Malweta; 8.3° N, 9.233° W; 18 Aug. 2003; V. Nicolas and M. Colyn; anthropogenic forest; GenBank no.: ON620408 (16S); MNHN, MNHN-ZM-2020-1895 • 1 ♀ adult; Yerende; 10.04° N, 13.68° W; 14 Mar. 2005; C. Denys and A. Lalis leg.; GenBank nos: MH806027 (Cytb), MH782821 (16S); MNHN, MNHN-ZM-2013-781.

Other material examined

GUINEA • 1 ♂ adult; Franfina; 9.63° N, 8.94° W; Feb. 2004; C. Denys and E. Lecompte leg.; GenBank nos: MH806022 (Cytb), MH782816 (16S); MNHN, MNHN-ZM-2013-769 • 1 ♀ adult; same data as for preceeding; GenBank nos: MH806023 (Cytb), MH782817 (16S); MNHN, MNHN-ZM-2013-770

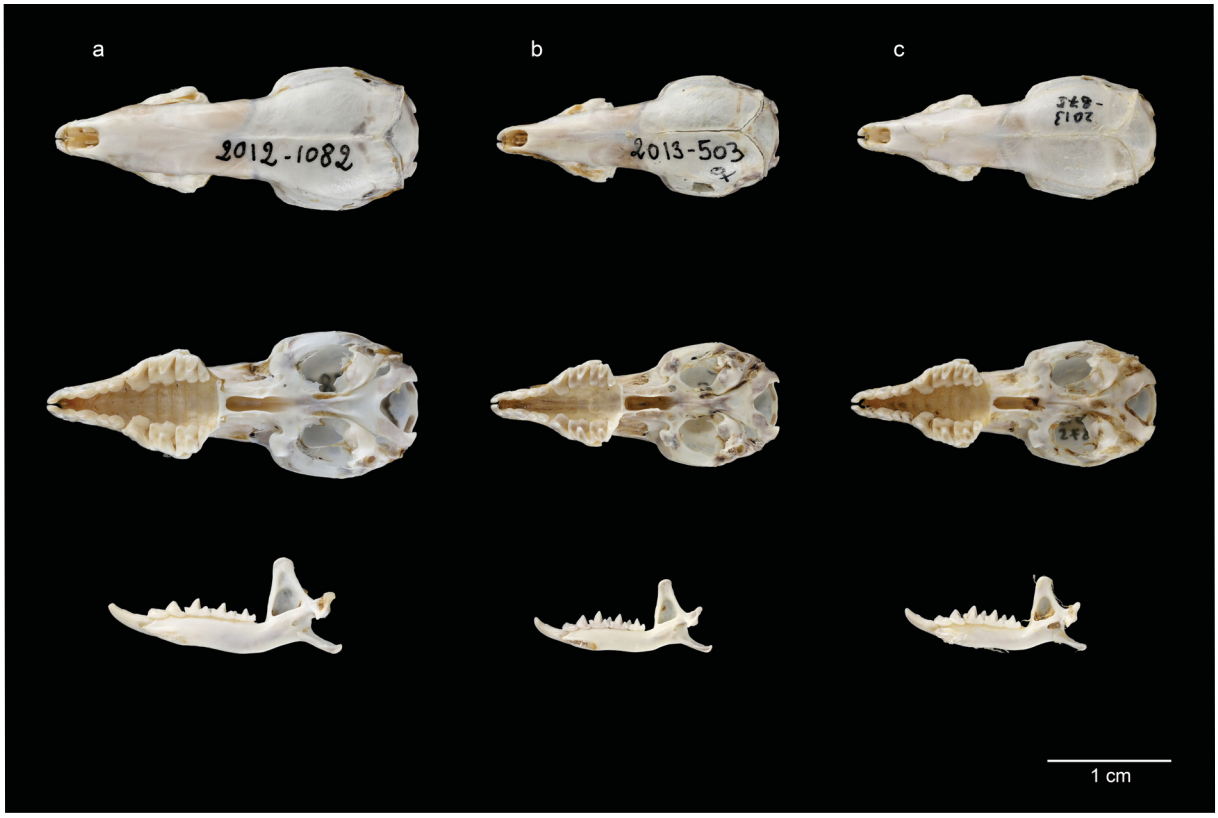

Fig. 7. SkullS in dorsal, ventral and lateral view and mandible. **a.** *Crocidura grandiceps* MNHN-ZM-2012-1082 **b.** *Crocidura pediculus* sp. nov. Voet, Cornette & Nicolas holotype, ♀ MNHN-ZM-2013-503 and **c.** *Crocidura* cf. *longipes* MNHN-ZM-2013-875. All images are standardized. Selected individuals are the closest to the morphospace centroid for the species.

• 1 ♀ adult ; same data as for preceeding; GenBank nos: ON603720 (Cytb), ON532738 (16S); MNHN, MNHN-ZM-2013-771 • 1 ♂ adult; Gbie; 7.640° N, 8.417° W; 406 m a.s.l.; Feb. 2008; C. Denys leg.; lowland forest; GenBank nos: JQ732363 (Cytb), JQ732590 (16S); MNHN, MNHN-ZM-2012-1077 • 1 ♀ adult ; Gbie; 7.642° N, 8.337° W; 467 m a.s.l.; Oct. 2008; C. Denys leg.; lowland forest; GenBank nos: JQ732393 (Cytb), JQ732626 (16S); MNHN, MNHN-ZM-2012-1079 • 1 ♀ adult; Hermakono; 9.036° N, 8.918° W; 680 m a.s.l.; 7 Aug. 2011; V. Nicolas and A. Lalis leg.; forest; GenBank nos: PX054675 (Cytb), PX633558 (complete mtDNA), PX054759 (ApoB), PX054793 (BRCA1), PX054813 (BDNF), PX054849 (GHR), PX054882 (HDAC2), PX054905 (MCGF), PX054936 (STAT5A), PX054960 (vWF); MNHN, MNHN-ZM-2013-449 • 1 ♂ young adult; Ziama forest, Kazaouma; 8.35° N, 9.217° W; 27 Aug. 2003; V. Nicolas and M. Colyn; fallow; GenBank no.: PX054649 (Cytb); MNHN, MNHN-ZM-2019-241 • 1 ♂ young adult; same locality as for preceeding; 19 Sep. 2003; V. Nicolas and M. Colyn; field; GenBank no.: PX057592 (16S); MNHN, MNHN-ZM-2024-997 • 1 ♂ subadult; same locality as for preceeding; 21 Sep. 2003; V. Nicolas and M. Colyn; fallow; GenBank nos: PX054733 (Cytb), MH782827 (16S); MNHN, MNHN-ZM-2024-998 • 1 ♀; same locality as for preceeding; 15 Oct. 2003; V. Nicolas and M. Colyn; fallow; GenBank nos: MH806034 (Cytb), MH782828 (16S); MNHN, MNHN-ZM-2024-999 • 1 ♂ adult; same locality as for preceeding; 21 Nov. 2003; V. Nicolas and M. Colyn; cornfield; GenBank nos: EF524681 (Cytb), EF524897 (16S); MNHN, MNHN-ZM-2024-1000 • 1 ♂ subadult; Ziama forest, Malweta; 8.3° N, 9.233° W; 28 Oct. 2003; V. Nicolas and M. Colyn; anthropogenic forest; GenBank nos: MH806035 (Cytb). MH782829 (16S); MNHN, MNHN-ZM-2024-1001 • 1 ♀ young adult; same locality as for preceeding; 12 Nov. 2003; V. Nicolas and M. Colyn; secondary forest; GenBank nos: MH806036 (Cytb). MH782830 (16S); MNHN, MNHN-ZM-2024-1002 • 1 ♀; Kediana; 11.82° N, 10.14° W; 14 Dec. 2011; C. Denys and A. Lalis leg.; GenBank nos: PX054703 (Cytb); MNHN, MNHN-ZM-2013-756 • 1 ♂; Yerende; 10.04° N, 13.68° W; 14 Mar. 2005; C. Denys and A. Lalis leg.; GenBank nos: PX054641 (Cytb), PX057594 (16S); MNHN, MNHN-ZM-2013-778 • 1 ♀; same data as for preceeding; GenBank nos: PX054704 (Cytb), PX057595 (16S); MNHN, MNHN-ZM-2013-779 • 1 ♂; same data as for preceeding; GenBank nos: MH806026 (Cytb), MH782820 (16S); MNHN, MNHN-ZM-2013-780 • 1 ♂; same data as for preceeding; GenBank nos: PX054642 (Cytb), PX057596 (16S); MNHN, MNHN-ZM-2013-782 • 1 ♀; same data as for preceeding; GenBank no.: PX057597 (16S); MNHN, MNHN-ZM-2013-783 • 1 ♂; same data as for preceeding; GenBank no.: PX057598 (16S); MNHN, MNHN-ZM-2013-784 • 1 ♀; same data as for preceeding; GenBank no.: PX057599 (16S); MNHN, MNHN-ZM-2013-786 • 1 ♀; same data as for preceeding; GenBank no.: PX054734 (Cytb), PX057593 (16S); MNHN, MNHN-ZM-2013-789 • 1 ♀; same data as for preceeding; GenBank nos: MH806028 (Cytb), MH782822 (16S); MNHN, MNHN-ZM-2013-790 • 1 ♂; same locality as for preceeding; 15 Mar. 2005; C. Denys and A. Lalis leg.; GenBank no.: PX057600 (16S); MNHN, MNHN-ZM-2013-787 • 1 ♂; same data as for preceeding; GenBank no.: PX057601 (16S); MNHN, MNHN-ZM-2013-788 • 1 ♀ adult; Zogota; 7.931° N, 9.125° W; 12 Jun. 2011; V. Nicolas and A. Lalis leg.; fallow; GenBank nos: PX054645 (Cytb), PX633555 (complete mtDNA), PX054756 (ApoB), PX054790 (BRCA1), PX054810 (BDNF), PX054846 (GHR), PX054879 (HDAC2), PX054902 (MCGF), PX054933 (STAT5A), PX054957 (vWF); MNHN, MNHN-ZM-2013-477.

LIBERIA • 1 ♂ adult; Fape; 7.242° N, 9.305° W; 14 Jul. 2011; V. Nicolas and A. Lalis leg.; forest; GenBank nos: PX054698 (Cytb), PX633556 (complete mtDNA), PX054757 (ApoB), PX054791 (BRCA1), PX054811 (BDNF), PX054847 (GHR), PX054880 (HDAC2), PX054903 (MCGF), PX054934 (STAT5A), PX054958 (vWF); MNHN, MNHN-ZM-2013-438 • 1 ♀ adult; Fape; 7.230° N, 9.300° W; 16 Jul. 2011; V. Nicolas and A. Lalis leg.; fallow; GenBank nos: PX054598 (Cytb), PX633557 (complete mtDNA), PX054758 (ApoB), PX054792 (BRCA1), PX054812 (BDNF), PX054848 (GHR), PX054881 (HDAC2), PX054904 (MCGF), PX054935 (STAT5A), PX054959 (vWF); MNHN, MNHN-ZM-2013-439 • 1 ♀; Fape; 7.226° N, 9.292° W; 10 Jul. 2011; V. Nicolas and A. Lalis leg.; backwater; GenBank nos: MH806040 (Cytb), MH782833 (16S); MNHN, MNHN-ZM-2013-495.

COTE D'IVOIRE • 1 ♂; Gbagroube; 5.85° N, 5.3° W; 12 Mar. 2005; S.; Kan Kouassi and B. Allali Kouadio leg.; GenBank no.: PX057568 (16S); MNHN, MNHN-ZM-2012-1474.

Description (see Figs 6–7 and SM2 Figs 5–6)

Crocidura pediculus sp. nov. has a dark brown color, with a slightly lighter belly, shifting to a slate brown, greyer than the back (Fig. 6). The transition between the back and belly coloring is gradual, with no defined delimitation. The tail is dark brown, nearly black, covered by hairs along its entire length. Hands and feet are brown, the outside darker than the inside. Ears are large, covered in very short hairs and appearing bald. Even if in external coloring *C. pediculus* looks like *C. grandiceps* they are very different based on morphometry. *Crocidura grandiceps* appears to have longer and larger limbs, an elongated head, a longer, wider tail, thicker at the base, and more numerous and thicker darker head vibrissae. All external measurements are significantly smaller in *C. pediculus* (weight = 13.06 ± 2.81 g, body length = 92.02 ± 9.00 mm, tail length = 58.95 ± 8.58 mm, hindfoot length = 15.02 ± 1.01 mm, and ear length = 8.32 ± 1.72 mm) than in *C. grandiceps* (weight = 19.07 ± 5.30 g, body length = 101.35 ± 8.67 mm, tail length = 77.46 ± 11.24 mm, hindfoot length = 19.11 ± 2.78 mm and ear length = 10.72 ± 1.89 mm; SM2 Fig. 6). These size differences between the two species are also apparent on the skull and the mandibles. *Crocidura grandiceps* has a more elongated rostrum and small braincase compared to *Crocidura pediculus*. Its palatine bone extends much further into the interorbital area.

Based on external body measurements, *Crocidura pediculus* sp. nov. resembles *C.* cf. *longipes*. However, their pelage coloration is different, *C. longipes* having been originally described as a uniformly chocolate brown shrew with very long hindfeet and a sparsely haired tail. The skull of *C. pediculus* is more globular, while it is more elongated in *C.* cf. *longipes*. The dentition is weaker in *C.* cf. *longipes* and the angular process of the mandible is longer in *C. pediculus*.

Crocidura pediculus sp. nov. differs significantly from *C. buettikoferi* in ear length, having smaller ears (8.32 ± 1.72 mm and 9.25 ± 1.81 mm, respectively). Morphometric analyses also reveal differences in skull shape (dorsal and ventral views), although *C. buettikoferi* occupies a central position in the morphospace for all three cranial structures. The braincase of *C. pediculus* is more globular and the rostrum shorter. The coloration of the pelage of *C. buettikoferi* is similar to that of *C. pediculus*: its dorsal pelage is deep-chocolate-brown and the ventral pelage is paler or greyish-brown. The tail is dark, very sparsely covered with hairs and bristles (pilosity ca 50%).

Crocidura pediculus sp. nov. and *C. therease* have similar external, skull or mandibular sizes, except the longer tail length (58.95 ± 8.58 mm) and hind foot length (15.02 ± 1.01 mm) of *C. therease* (53.63 ± 4.46 mm and 14.185 ± 1.18 mm, respectively). These species also have very similar skull and mandibles shapes. However, they can be discriminated based on coloration: *C. theresae* is a small-sized shrew described as lighter in color than the other WA species from the complex *C. poensis*, with a greyish coloring and light grey belly. The feet and tail are shorter. The tail has sparse brown hairs, pilosity ca 75%.

Crocidura wimmeri is a rare, critically endangered shrew species (Vogel *et al.* 2014) and we only had two specimens in our dataset. Thus, we were not able to compare it morphometrically to *C. pediculus* sp. nov. *Crocidura wimmeri* is a medium-sized species, and its coat is almost uniformly dark ash-grey, with only a brown sheen on the dorsal side. The tail is not densely haired.

No genotyped specimens of *C. foxi* can be found west of the Dahomey gap, which should exclude the confusion between the two species as there is probably no geographic overlap in their geographic ranges.

Ecology and distribution

Crocidura pediculus sp. nov. is a habitat generalist, captured mostly in primary lowland forests, fields and young fallows. One individual was captured in an anthropogenic forest and one in wetlands.

The current distribution of known specimens is Guinea and Liberia and extends to Ivory Coast, with a single specimen captured in Gbagroube, in the center of the country.

Discussion

Genetic analyses

In *Crocidura* shrews, the mean genetic distance between sister species using Cytb sequences typically exceeds 6% (Bannikova *et al.* 2011; Jacquet *et al.* 2012; Jacquet *et al.* 2014). *Crocidura pediculus* sp. nov. displays similar values of genetic distance with all other species except between itself and its closest mitochondrial relative, *C. grandiceps* (2.6%). Although unusual, similar cases have been previously reported between other shrew species (Jacquet *et al.* 2015). The value between itself and its second closest mitochondrial relative *C.* cf. *longipes* is on the lower end of the spectrum, but still included in it (6.2%). Species discrimination analyses based on Cytb sequences and barcode gaps directly reflect this result, as ASAP's best partition fails to discriminate between *C. grandiceps* and *C. pediculus*. However it partitions the four *C. wimmeri* sequences in two distinct lineages, from Ghana and Ivory Coast, suggesting the existence of a cryptic species. Since *C. wimmeri* is rare and considered as endangered, few specimens are available for analysis and this result could not be further investigated. The use of single mitochondrial markers (barcodes) is useful for many species delimitations, but is not sufficient in certain cases, over or underestimating the number of species (Esquivel *et al.* 2022; Penna *et al.* 2022). Furthermore, the mitochondrial and nuclear DNA datasets do not output exactly the same results. The complete mitogenome ML and Bayesian trees display the same results as the Cytb approximate-ML tree, supporting the monophyly of *C. pediculus,* and placing it as the closest relative to *C. grandiceps*. Those two are in turn the closest relatives of *C.* cf. *longipes*, with strong support. ASAP's best partition for the complete mitogenome retrieves *C. pediculus* and *C. grandiceps* as separate species. Since shrews are short-lived, it has been suggested that they might have higher rates of molecular evolution (Esselstyn & Brown 2009), but this may not be the case for all species, depending on the strength of selection and drift, and low levels of genetic distance have been detected between recognized species (Jacquet *et al.* 2015). As in Nicolas *et al*. (2019), the concatenated nuclear DNA ML and Bayesian approaches fail to retrieve the monophyly of *C. pediculus*, gathering all three closest relatives *C. grandiceps, C.* cf. *longipes* and *C. pediculus* in a single group. The dated species tree reconstructed in Voet *et al*. (2022) placed *C. pediculus* as a sister species to *C. grandiceps*, as does the mitochondrial tree. This may result from the disequilibrium between the number of mitochondrial and nuclear sites. The divergence between the two species was estimated at around 350 ky, representing a very recent split on evolutionary timescales. As mitochondrial DNA evolves four times faster than nuclear DNA, it is not unusual to encounter mitochondrial monophyly along with an unresolved nuclear phylogeny (Toews & Brelsford 2012; Després 2019). The BPP analyses produce similar results with all three datasets, the five independent runs supporting the seven species hypothesis (i.e., validating *C. pediculus* as a distinct species) and outputting posterior probability values of 1 or near 1 for all seven tested species. The nuclear species tree portrays *C.* cf. *longipes* as a closest relative to *C. pediculus* with moderate support (0.90), whereas the maximum clade credibility tree based on the mitogenome portrays *C. grandiceps* and *C. pediculus* as sisters. Which represents the closest relative to *C. pediculus* therefore remains uncertain. The discordance between mitochondrial and nuclear DNA is a common phenomenon in animals (Rabone *et al.* 2015; Naidoo *et al.* 2016). Studies have found several potential causes, ranging from adaptive introgression of mitochondrial DNA to demographic disparities such as sex-biased asymmetries, incomplete lineage sorting and hybrid zone movements. In lineages where divergent mitochondrial clades have emerged without geographic isolation, which may have been the case here, adaptive introgression and sex-biased

asymmetries are the favoured hypotheses (Toews & Brelsford 2012). In mammals, different dispersal abilities between males and females is widespread, females often being more sedentary than males (Li & Kokko 2019). Shrews appear to be no exception and many species are considered as highly territorial (Wilson & Mittermeier 2018), which may explain the discrepancy despite the lack of knowledge about the lifestyles of the shrews of the *C. poensis* species complex. However, many authors discuss sex-biased dispersal and argue that it generates high levels of mitochondrial divergence (Després 2019). Here, mitochondrial divergence between *C. grandiceps* and *C. pediculus* is low, despite lineage monophyly, possibly discarding sex-biased dispersal as a driver. Genome scale data are needed to further investigate the nuclear difference between *C. grandiceps, C. pediculus* and *C.* cf. *longipes*.

Morphology

Nearly all individuals in the museum collections genetically identified as being *C. pediculus* sp. nov. were initially attributed the name *C. grandiceps*. However, *C. pediculus* and *C. grandiceps* are among the most morphologically different in the species complex, displaying significant differences in size and shape in all three examined structures, and in all recorded external body measurements. The very similar coloring, and overlapping geographic ranges may explain the difficulty in differentiating them. However, multiple morphometrical differences are found between the two species (see species description).

A few individuals of *C. pediculus* sp. nov. have been initially morphologically identified in museum collections as *C. buettikoferi* or *C. foxi*. No genotyped specimens of *C. foxi* can be found west of the Dahomey gap, which should eliminet the confusion as there is probably little to no geographic overlap in their ranges. *Crocidura pediculus* differs significantly from *C. buettikoferi* in ear length, having smaller ears, and in skull shape (dorsal and ventral views). *Crocidura pediculus* is most similar in external measurements and skull and mandible size and shape to *C. theresae* and *C.* cf. *longipes,* yet no confusions have been made in museum collections, probably due to their distinct coloration.

New species versus morphotype

Through the comparison of the genetic and morphological material available for numerous specimens of the *C. poensis* species complex, we propose to consider *C. pediculus* sp. nov. as a new species. Some confusion remains regarding the relationships between the closely related *C. grandiceps*, *C. pediculus* and *C.* cf. *longipes*, whether due to incomplete lineage sorting and/or the choice of nuclear markers, or mito/nuclear introgression. Despite the nuclear ML and Bayesian trees failing to retrieve the monophyly of *C. pediculus*, the BPP analyses on both the mitochondrial and nuclear DNA output higher support for the seven species hypothesis. Lastly, and despite this apparent recent speciation event and low mitochondrial divergence, there is strong morphological divergence between *C. grandiceps* and *C. pediculus*, which remains rare among *Crocidura* shrews (Esselstyn *et al*. 2021; Hinckley *et al*. 2022). In the skull of *C. grandiceps* and *C. pediculus*, the divergence seems to have occurred mainly in rostrum length and robustness. This has been observed in other speciose groups such as bats, where many morphotypes have evolved according to a variety of diets (Hedrick *et al*. 2020). Morphological disparity within the former *C. grandiceps* species reached twice the values within other species, questioning even its denomination as cryptic species (Voet *et al*. 2022). Cryptic species usually refer to species that are morphologically unidentifiable and rely on genetic markers to be discriminated (Fišer *et al*. 2018; Struck *et al*. 2018; Korshunova *et al*. 2019). Here, crypsis remains only in the historical sense, as they were initially grouped under the same species name. Morphologically speaking, *C. pediculus* is much smaller than *C. grandiceps* and can be statistically discriminated from its former namesake. Its measurements (skull and body) resemble those of the open-habitat dweller and more distant relative *C. theresae*. The diversification of West African *C. poensis* complex species may have been driven by both Pleistocene refuge dynamics and divergent selection across ecological gradients (Nicolas *et al*. 2019). Habitat preferences within the complex reveal distinct niche partitioning: *C. buettikoferi* occupies a wide range of habitats, including grasslands within the rain forest, forests, relict forests in derived savanna, fallows

and cocoa plantations; *C. grandiceps* is considered a forest species; *C. theresae* primarily inhabits open habitats such as grasslands and fields, with rare occurrences in forest relicts; *C. wimmeri* is restricted to wet, swampy coastal forest in eastern Ivory Coast and western Ghana; *C.* cf. *longipes* is confined to isolated gallery forests in western coastal Guinea. Notably, over half of the*C. pediculus* specimens were captured in open habitats (fields and fallows), suggesting character displacement with the forest-dwelling species *C. grandiceps* (Brown & Wilson 1956; Fišer *et al*. 2015; Biedma *et al*. 2020) or evolutionary convergence with the open-habitat species *C. theresae*, potentially linked to habitat preferences and predator evasion (Spaeth 2009; Zou & Zhang 2016). Further work is necessary in order to improve our comprehension of the relationships within the *C. poensis* species complex, but also on the processes responsible for its diversification. To this aim coupled phenotypic and genome wide approaches allowing the detection of signatures of natural selection would be useful.

Acknowledgments

This work was supported by the "Action Transversale du Muséum 2017" (CROCIDURA project), the "Projet fédérateur du département Origines et Evolution 2020" (COLLCROC project). Molecular lab work was performed at the "Service de Systématique Moléculaire" (UMS 2700 2AD, Muséum National d'Histoire Naturelle, Paris, France). IV was funded by a doctoral fellowship of the doctoral school ED227. Our thanks go to the field collectors responsible for acquiring the specimens included in this study: Marc Colyn, Alain-Didier Missoup, Elisabeth Fichet-Calvet, Emilie Lecompte, Fodé Kourouma, Patrick Barrière, Stéphane Kan Kouassi and Vladimir Aniskin. We thank Ondřej Mikula for his assistance with the use of BPP and the interpretation of results.

Author contributions

CD, AL, and VN made substantial contributions to specimen acquisition. AD prepared the skulls and contributed to pictures acquisition. IV photographed the specimens and conducted the morphometrics study. IV and VN performed molecular lab work. IV, RC, and VN took part in the design of the study and the interpretation of its results, and were involved in the drafting of the manuscript. All authors approved the final version of the manuscript.

Data availability

All sequences were uploaded to GenBank and accession numbers are available in SM1. A TPS file containing all specimens and their landmarks and a file with complete mtDNA sequence data with annotations have been uploaded to https://data.indores.fr/ (https://doi.org/10.48579/PRO/GCV4IT).

References

Adams D.C. & Otárola-Castillo E. 2013. Geomorph: an R package for the collection and analysis of geometric morphometric shape data. *Methods in Ecology and Evolution* 4: 393–399. https://doi.org/10.1111/2041-210X.12035

Amori G., Di Bagno E. & Luiselli L. 2021. Patterns of diversity, species richness and community structure in West African savannah small mammals (rodents and shrews). *Tropical Zoology* 34: 72–91. https://doi.org/10.4081/tz.2021.110

Bannikova A.A., Abramov A.V., Borisenko A.V., Lebedev V.S. & Rozhnov V.V. 2011. Mitochondrial diversity of the white-toothed shrews (Mammalia, Eulipotyphla, *Crocidura*) in Vietnam. *Zootaxa* 2812: 1–20. https://doi.org/10.11646/zootaxa.2812.1.1

Biedma L., Calzada J., Godoy J.A. & Román J. 2020. Local habitat specialization as an evolutionary response to interspecific competition between two sympatric shrews. *Journal of Mammalogy* 101: 80–91. https://doi.org/10.1093/jmammal/gyz203

Bohoussou K.H., Cornette R., Akpatou B., Colyn M., Kerbis Peterhans J., Kennis J., Šumbera R., Verheyen E., N'Goran E., Katuala P. & Nicolas V. 2015. The phylogeography of the rodent genus *Malacomys* suggests multiple Afrotropical Pleistocene lowland forest refugia. *Journal of Biogeography* 42: 2049–2016. https://doi.org/10.1111/jbi.12570

Bookstein F.L. 1991. *Morphometric tools for landmark data: geometry and biology*. Cambridge University Press, Cambridge.

Brown W.L. & Wilson E.O. 1956. Character displacement. *Systematic Biology* 5: 49–64. https://doi.org/10.2307/2411924

Ceríaco L.M.P., Marques M.P., Jacquet F., Nicolas V., Colyn M., Denys C., Sardinha P.C. & Bastos-Silveira C. 2015. Description of a new endemic species of shrew (Mammalia, Soricomorpha) from Príncipe Island (Gulf of Guinea). *Mammalia* 79: 325–341. https://doi.org/10.1515/mammalia-2014-0056

Churchfield S., Barrière P., Hutterer R. & Colyn M. 2004. First results on the feeding ecology of sympatric shrews (Insectivora: Soricidae) in the Taï National Park, Ivory Coast. *Acta Theriologica* 49: 1–15. https://doi.org/10.1007/BF03192504

CILSS. 2016. *Landscapes of West Africa – A Window on a Changing World*. U.S. Geological Survey EROS, Garretson.

Collyer M. & Adams D.C. 2021. RRPP: linear model evaluation with randomized residuals in a permutation procedure. Ver. 1.0.0. Available from https://github.com/mlcollyer/RRPP [accessed 5 May 2022].

Cooke S.B. & Terhune C.E. 2015. Form, Function, and Geometric Morphometrics. *The Anatomical Record* 298: 5–28. https://doi.org/10.1002/ar.23065

Cornette R., Tresset A. & Herrel A. 2015a. The shrew tamed by Wolff's law: Do functional constraints shape the skull through muscle and bone covariation? *Journal of Morphology* 276: 301–309. https://doi.org/10.1002/jmor.20339

Cornette R., Tresset A., Houssin C., Pascal M. & Herrel A. 2015b. Does bite force provide a competitive advantage in shrews? The case of the greater white-toothed shrew. *Biological Journal of the Linnean Society* 114: 795–807. https://doi.org/10.1111/bij.12423

Craig E.W., Bryjová A., Bryja J., Meheretu Y., Lavrenchenko L.A. & Kerbis Peterhans J.C. 2025. Integrative taxonomic revision of endemic dwarf shrews from the Ethiopian Highlands. *Journal of Vertrebrate Biology* 74: 25031. https://doi.org/10.25225/jvb.25031

deMenocal P.B. 2004. African climate change and faunal evolution during the Pliocene-Pleistocene. *Earth and Planetary Science Letters* 220: 3–24. https://doi.org/10.1016/S0012-821X(04)00003-2

Denys C., Jacquet F., Kadjo B., Missoup A.D., Aniskine V., Goüy de Bellocq J., Soropogui B., Douno M., Sylla M., Nicolas V., Lalis A. & Monadjem A. 2021. Shrews (Mammalia, Eulipotyphla) from a biodiversity hotspot, Mount Nimba (West Africa), with a field identification key to species. *Zoosystema* 43: 729–757. https://doi.org/10.5252/zoosystema2021v43a30

Després L. 2019. One, two or more species? Mitonuclear discordance and species delimitation. *Molecular Ecology* 28: 3845–3847. https://doi.org/10.1111/mec.15211

Dubey S., Salamin N., Ruedi M., Barriere P., Colyn M. & Vogel P. 2008. Biogeographic origin and radiation of the Old World crocidurine shrews (Mammalia: Soricidae) inferred from mitochondrial and nuclear genes. *Molecular Phylogenetics and Evolution* 48: 953–963. https://doi.org/10.1016/j.ympev.2008.07.002

Esquivel D.A., Pereira M.J.R., Stuhler J.D., Rossoni D.M., Velazco P.M. & Bianchi F.M. 2022. Multiples lines of evidence unveil cryptic diversity in the *Lophostoma brasiliense* (Chiroptera: Phyllostomidae) complex. *Systematics and Biodiversity* 20: 2110172. https://doi.org/10.1080/14772000.2022.2110172

Esselstyn J.A. & Brown R.M. 2009. The role of repeated sea-level fluctuations in the generation of shrew (Soricidae: *Crocidura*) diversity in the Philippine Archipelago. *Molecular Phylogenetics and Evolution* 53: 171–181. https://doi.org/10.1016/j.ympev.2009.05.034

Esselstyn J.A., Setiawan Achmadi A., Handika H., Swanson T., Giarla T.C. & Rowe K.C. 2021. Fourteen new, endemic species of shrew (genus *Crocidura*) from Sulawesi reveal a spectacular island radiation. *Bulletin of the American Museum of Natural History* 454: 1–108. https://doi.org/10.1016/j.ympev.2009.05.034

Fedosov A., Achaz G., Gontchar A. & Puillandre N. 2022. MOLD, a novel software to compile accurate and reliable DNA diagnoses for taxonomic descriptions. *Molecular Ecology Ressources* 22: 2038–2053. https://doi.org/10.1111/1755-0998.13590

Fišer C., Luštrik R., Sarbu S., Flot J.-F. & Trontelj P. 2015. Morphological evolution of coexisting Amphipod species pairs from Sulfidic caves suggests competitive interactions and character displacement, but no environmental filtering and convergence. *PLoS ONE* 10: e0123535. https://doi.org/10.1371/journal.pone.0123535

Fišer C., Robinson C.T. & Malard F. 2018. Cryptic species as a window into the paradigm shift of the species concept. *Molecular ecology* 27: 613–635. https://doi.org/10.1111/mec.14486

Gunz P. & Mitteroecker P. 2013. Semilandmarks: a method for quantifying curves and surfaces. *Hystrix-Italian Journal of Mammalogy* 24: 103–109. https://doi.org/10.4404/hystrix-24.1-6292

Hassanin A., Khouider S., Gembu G.C., Goodman S. M., Kadjo B., Nesi N., Pourrut X., Nakoune E. & Bonillo C. 2015. The comparative phylogeography of fruit bats of the tribe Scotonycterini (Chiroptera, Pteropodidae) reveals cryptic species diversity related to African Pleistocene forest refugia. *Comptes Rendus Biologies* 338: 197–211. https://doi.org/10.1016/j.crvi.2014.12.003

Hedrick B.P., Mutumi G.L., Munteanu V.D., Sadier A., Davies K.T.J., Rossiter S.J., Sears K.E., Dávalos L.M. & Dumont E. 2020. Morphological Diversification under High Integration in a Hyper Diverse Mammal Clade. *Journal of Mammalian Evolution* 27: 563–575. https://doi.org/10.1007/s10914-019-09472-x

Heubes J., Kühn I., König K., Wittig R., Zizka G. & Hahn K. 2011. Modelling biome shifts and tree cover change for 2050 in West Africa. *Journal of Biogeography* 38: 2248-2258. https://doi.org/10.1111/j.1365-2699.2011.02560.x

Hinckley A., Camacho-Sanchez M., Ruedi M., Hawkins M.T.R., Mullon M., Cornellas A., Tuh Yit Yuh F. & Leonard J.A. 2022. Evolutionary history of Sundaland shrews (Eulipotyphla: Soricidae: *Crocidura*) with a focus on Borneo. *Zoological Journal of the Linnean Society* 194: 478–501. https://doi.org/10.1093/zoolinnean/zlab045

Hoang D.T., Chernomor O., von Haeseler A., Minh B.Q. & Vinh L.S. 2018. UFBoot2: Improving the Ultrafast Bootstrap Approximation. *Molecular Biology and Evolution* 35: 518–522. https://doi.org/10.1093/molbev/msx281

Hutterer R. & Happold D.C.D. 1983. The shrews of Nigeria (Mammalia: Soricidae). *Bonner Zoologische Monographien* 18: 5–79.

Jacquet F., Nicolas V., Bonillo C., Cruaud C. & Denys C. 2012. Barcoding, molecular taxonomy and exploration of the diversity of shrews (Soricomorpha: Soricidae) on Mount Nimba (Guinea). *Zoological Journal of the Linnean Society* 166: 672–687. https://doi.org/10.1111/j.1096-3642.2012.00856.x

Jacquet F., Nicolas V., Colyn M., Kadjo B., Hutterer R., Akpatou B., Cruaud C. & Denys C. 2014. Forest refugia and riverine barriers promote diversification in the West African pygmy shrew (*Crocidura obscurior* complex, Soricomorpha). *Zoologica Scripta* 43: 131–148. https://doi.org/10.1111/zsc.12039

Jacquet F., Denys C., Verheyen E., Bryja J., Hutterer R., Kerbis Peterhans J.C., Stanley W.T., Goodman S.M., Couloux A., Colyn M. & Nicolas V. 2015. Phylogeography and evolutionary history of the *Crocidura olivieri* complex (Mammalia, Soricomorpha): from a forest origin to broad ecological expansion across Africa. *BMC Evolutionary Biology* 15: 71. https://doi.org/10.1186/s12862-015-0344-y

Jiao X., Flouri T. & Yang Z. 2021. Multispecies coalescent and its applications to infer species phylogenies and cross-species gene flow. *National Science Review* 8: nwab127. https://doi.org/10.1093/nsr/nwab127

Kearse M., Moir R., Wilson A., Stones-Havas S., Cheung M., Sturrock S., Buxton S., Cooper A., Markowitz S., Duran C., Thierer T., Ashton B., Meintjes P. & Drummond A. 2012. Geneious Basic: an integrated and extendable desktop software platform for the organization and analysis of sequence data. *Bioinformatics* 28: 1647–1649. https://doi.org/10.1093/bioinformatics/bts199

Konečný A., Hutterer R., Meheretu Y. & Bryja J. 2020. Two new species of *Crocidura* (Mammalia: Soricidae) from Ethiopia and updates on the Ethiopian shrew fauna. *Journal of Vertebrate Biology* 69: 20064.20061–20016. https://doi.org/10.25225/jvb.20064

Korshunova T., Picton B., Furfaro G., Mariottini P., Pontes M., Prkić J., Fletcher K., Malmberg K., Lundin K. & Martynov A. 2019. Multilevel fine-scale diversity challenges the 'cryptic species' concept. *Scientific Reports* 9: 6732. https://doi.org/10.1038/s41598-019-42297-5

Kumar S., Stecher G. & Tamura K. 2016. MEGA7: Molecular Evolutionary Genetics Analysis Version 7.0 for Bigger Datasets. *Molecular Biology and Evolution* 33: 1870–1874. https://doi.org/10.1093/molbev/msw054

Lanfear R., Frandsen P.B., Wright A.M., Senfeld T. & Calcott B. 2017. PartitionFinder 2: New methods for selecting partitioned models of evolution for molecular and morphological phylogenetic analyses. *Molecular Biology and Evolution* 34: 772–773. https://doi.org/doi:10.1093/molbev/msw260

Li X.-Y. & Kokko H. 2019. Sex-biased dispersal: a review of the theory. *Biological Reviews* 94: 721–736. https://doi.org/10.1111/brv.12475

Mamba M.L., Dalton D.L., Mahlaba T.A.M., Kropff A.S. & Monadjem A. 2021. Small mammals of a West African hotspot, the Ziama-Wonegizi-Wologizi transfrontier forest landscape. *Mammalia* 85: 127–144. https://doi.org/10.1515/mammalia-2020-0013

Naidoo T., Schoeman M.C., Goodman S.M., Taylor P.J. & Lamb J.M. 2016. Discordance between mitochondrial and nuclear genetic structure in the bat *Chaerephon pumilus* (Chiroptera: Molossidae) from southern Africa. *Mammalian Biology* 81: 115–122. https://doi.org/10.1016/j.mambio.2015.11.002

Needham A.E. & Hardy A.C. 1950. The form-transformation of the abdomen of the female pea-crab, *Pinnotheres pisum* Leach. *Proceedings of the Royal Society of London. Series B - Biological Sciences* 137: 115–136. https://doi.org/10.1098/rspb.1950.0027

Nguyen L.T., Schmidt H.A., von Haeseler A. & Minh B.Q. 2015. IQ-TREE: A Fast and Effective Stochastic Algorithm for Estimating Maximum-Likelihood Phylogenies. *Molecular Biology and Evolution* 32: 268–274. https://doi.org/10.1093/molbev/msu300

Nicolas V., Jacquet F., Hutterer R., Konečný A., Kan Kouassi S., Durnez L., Lalis A., Colyn M. & Denys C. 2019. Multi-locus phylogeny of the *Crocidura poensis* species complex (Mammalia, Soricomorpha): influences of the paleoclimate on its diversification and evolution. *Journal of Biogeography* 46: 871–883. https://doi.org/10.1111/jbi.13534

Nicolas V., Fabre P.-H., Bryja J., Denys C., Verheyen E., Missoup A.D., Olayemi A., Katuala P., Dudu A., Colyn M., Peterhans J.K. & Demos T. 2020. The phylogeny of the African wood mice (Muridae, *Hylomyscus*) based on complete mitochondrial genomes and five nuclear genes reveals their evolutionary history and undescribed diversity. *Molecular Phylogenetics and Evolution* 144: 106703. https://doi.org/10.1016/j.ympev.2019.106703

Nosil P. 2012. *Ecological Speciation*. Oxford University Press, Oxford.

Padial J.M., Miralles A., De la Riva I. & Vences M. 2010. The integrative future of taxonomy. *Frontiers in zoology* 7: 16. https://doi.org/10.1186/1742-9994-7-16

Penna A., Dillon R., Bearder S.K., Karlsson J., Perkin A. & Pozzi L. 2022. Phylogeography and evolutionary lineage diversity in the small-eared greater galago, *Otolemur garnettii* (Primates: Galagidae). *Zoological Journal of the Linnean Society*: 198 (1): 131–148. https://doi.org/10.1093/zoolinnean/zlac079

Price M.N., Dehal P.S. & Arkin A.P. 2010. FastTree 2 – Approximately Maximum-Likelihood Trees for Large Alignments. 5: e9490. https://doi.org/10.1371/journal.pone.0009490

Puillandre N., Brouillet S. & Achaz G. 2021. ASAP: assemble species by automatic partitioning. *Molecular Ecology Resources* 21: 609–620. https://doi.org/10.1111/1755-0998.13281

R Core Team. 2021. R: A language and environment for statistical computing. Foundation for Statistical Computing. Available from https://www.R-project.org/ [accessed 10 Jan. 2022].

Rabone M., Lavery S.D., Little A. & Clements K.D. 2015. Discordance between nuclear and mitochondrial DNA analyses of population structure in closely related triplefin fishes (*Forsterygion lapillum* and *F. capito*, F. Tripterygiidae) supports speciation with gene flow. *Marine Biology* 162: 1611–1624. https://doi.org/10.1007/s00227-015-2697-6

Rambaut A., Drummond A.J., Xie D., Baele G. & Suchard M.A. 2018. Posterior summarization in Bayesian phylogenetics using Tracer 1.7. *Systematic Biology* 67: 901–904. https://doi.org/10.1093/sysbio/syy032

Rannala B. & Yang Z. 2003. Bayes estimation of species divergence times and ancestral population sizes using DNA sequences from multiple loci. *Genetics* 164: 1645–1656. https://doi.org/10.1093/genetics/164.4.1645

Rohlf F.J. 2005. *tpsDig, digitize landmarks and outlines, version 2.05*. State University of New York-Department of Ecology and Evolution, Stony Brook.

Rohlf F.J. & Slice D. 1990. Extensions of the Procrustes method for the optimal superimposition of landmarks. *Systematic Zoology* 39: 40–59. https://doi.org/10.2307/2992207

Ronquist F. & Huelsenbeck J.P. 2003. MrBayes 3: Bayesian phylogenetic inference under mixed models. *Bioinformatics* 19: 1572–1574. https://doi.org/10.1093/bioinformatics/btg180

Schlager S., Jefferis G. & Ian D. 2020. Morpho: calculations and visualisations related to geometric morphometrics. Ver. 2.8. Available from https://CRAN.R-project.org/package=Morpho. [accessed 5 May 2022]

Spaeth P.A. 2009. Morphological convergence and coexistence in three sympatric North American species of *Microtus* (Rodentia: Arvicolinae). *Journal of Biogeography* 36: 350–361. https://doi.org/10.1111/j.1365-2699.2008.02015.x

Srivathsan A. & Meier R. 2012. On the inappropriate use of Kimura-2-parameter (K2P) divergences in the DNA-barcoding literature. *Cladistics* 28: 190–194. https://doi.org/10.1111/j.1096-0031.2011.00370.x

Struck T.H., Feder J.L., Bendiksby M., Birkeland S., Cerca J., Gusarov V.I., Kistenich S., Larsson K.H., Liow L.H., Nowak M.D., Stedje B., Bachmann L. & Dimitrov D. 2018. Finding Evolutionary Processes Hidden in Cryptic Species. *Trends in Ecology and Evolution* 33: 153–163. https://doi.org/10.1016/j.tree.2017.11.007

Toews D.P. & Brelsford A. 2012. The biogeography of mitochondrial and nuclear discordance in animals. *Molecular Ecology* 21: 3907–3930. https://doi.org/10.1111/j.1365-294X.2012.05664.x

Trauth M.H., Larrasoana J.C. & Mudelsee M. 2009. Trends, rhythms and events in Plio-Pleistocene African climate. *Quaternary Science Reviews* 28: 399–411. https://doi.org/10.1016/j.quascirev.2008.11.003

Voet I., Denys C., Colyn M., Lalis A., Konečný A., Delapré A., Nicolas V. & Cornette R. 2022. Incongruences between morphology and molecular phylogeny provide an in sight into the diversification of the *Crocidura poensis* species complex. *Scientific Reports* 12: e10531. https://doi.org/10.1038/s41598-022-12615-5

Vogel P., Vogel V., Fumagalli L., Kadjo K., Kouadio R.Y. & Dubey S. 2014. Genetic identity of the critically endangered Wimmer's shrew *Crocidura wimmeri*. *Biological Journal of the Linnean Society* 111: 224–229. https://doi.org/10.1111/bij.12196

Wilson D.E. & Mittermeier R.A. 2018. *Handbook of the Mammals of the World, Volume 8. Insectivores, Sloths and Colugos*. Lynx Edicions, Barcelona.

Yang Z. 2015. The BPP program for species tree estimation and species delimitation *Current Zoology* 61: 854–865. https://doi.org/10.1093/czoolo/61.5.854

Zhen Y., Harrigan R.J., Ruegg K.C., Anderson E.C., Ng T.C., Lao S., Lohmueller K.E. & Smith T.B. 2017. Genomic divergence across ecological gradients in the Central African rainforest songbird (*Andropadus virens*). *Molecular Ecology* 26: 4966–4977. https://doi.org/10.1111/mec.14270

Zou Z. & Zhang J. 2016. Morphological and molecular convergences in mammalian phylogenetics. *Nature Communications* 7: e12758. https://doi.org/10.1038/ncomms12758

Printed versions of all papers are deposited in the libraries of two of the institutes that are members of the EJT consortium: Muséum national d'Histoire naturelle, Paris, France and Royal Museum for Central Africa, Tervuren, Belgium. The other members of the consortium are: Royal Belgian Institute of Natural Sciences, Brussels, Belgium; Meise Botanic Garden, Meise, Belgium; Natural History Museum of Denmark, Copenhagen, Denmark; Naturalis Biodiversity Center, Leiden, the Netherlands; Museo Nacional de Ciencias Naturales-CSIC, Madrid, Spain; Leibniz Institute for the Analysis of Biodiversity Change, Bonn – Hamburg, Germany; National Museum of the Czech Republic, Prague, Czech Republic; The Steinhardt Museum of Natural History, Tel Aviv, Israël.

Supplementary files.

Suppl. file 1. List of specimens used in the present study with information on their geographic origin, date of collection, collector, GenBank accession numbers, sex, age, external measurements and the analyses in which they were used. https://doi.org/10.5852/ejt.2026.1039.3197.14191

Suppl. file 2. Supplementary tables and figures. https://doi.org/10.5852/ejt.2026.1039.3197.14193